

1 Validation of 10-year SAO OMI Ozone Profile (PROFOZ)

2 Product Using Ozonesonde Observations

3
4 Guanyu Huang^{1,*}, Xiong Liu¹, Kelly Chance¹, Kai Yang², Pawan K. Bhartia³, Zhaonan Cai¹,
5 Marc Allaart⁴, Gérard Ancellet⁵, Bertrand Calpini⁶, Gerrie J. R. Coetzee⁷, Emilio Cuevas-
6 Agulló⁸, Manuel Cupeiro⁹, Hugo De Backer¹⁰, Manvendra K. Dubey¹¹, Henry E. Fuelberg¹²,
7 Masatomo Fujiwara¹³, Sophie Godin-Beekmann⁵, Tristan J. Hall¹², Bryan Johnson¹⁴, Everette
8 Joseph¹⁵, Rigel Kivi¹⁶, Bogumil Kois¹⁷, Ninong Komala¹⁸, Gert König-Langlo¹⁹, Giovanni
9 Laneve²⁰, Thierry Leblanc²², Marion Marchand, Kenneth R. Minschwaner²³, Gary Morris²⁴,
10 Michael J. Newchurch²⁵, Shin-Ya Ogino²⁶, Nozomu Ohkawara²⁷, Ankie J. M. PETERS⁴, Françoise
11 Posny²⁸, Richard Querel²⁹, Rinus Scheele⁴, Frank J. Schmidlin³, Russell C. Schnell¹⁴, Otto
12 Schrems¹⁹, Henry Selkirk³⁰, Masato Shiotani³¹, Pavla Skrivánková³², René Stübi⁶, Ghassan
13 Taha³⁰, David W. Tarasick³³, Anne M. Thompson³, Valérie Thouret³⁴, Matt Tully³⁵, Roeland
14 van Malderen¹⁰, , Holger Vömel³⁶, Peter von der Gathen³⁷, Jacquelyn C. Witte³⁸, Margarita
15 Yela³⁹

- 16 1. Harvard-Smithsonian Center for Astrophysics, Cambridge, MA, USA
- 17 2. Department of Atmospheric and Oceanic Science, University of Maryland, College Park,
18 Maryland, USA
- 19 3. NASA Goddard Space Flight Center, Greenbelt, Maryland, USA
- 20 4. Royal Netherlands Meteorological Institute (KNMI), De Bilt, the Netherlands
- 21 5. LATMOS-ISPL, Université Paris 6 Pierre-et-Marie-Curie, Paris, France
- 22 6. MeteoSwiss Aerological Station, Federal Office of Meteorology and Climatology
23 MeteoSwiss, Payerne, Switzerland
- 24 7. South African Weather Service, Pretoria, South Africa
- 25 8. Izana Atmospheric Research Center, Meteorological State Agency of Spain, Santa Cruz de
26 Tenerife, Spain
- 27 9. National Meteorological Service, Ushuaia, Tierra del Fuego, Argentina
- 28 10. Royal Meteorological Institute of Belgium, Brussel, Belgium
- 29 11. Los Alamos National Laboratory, Los Alamos, NM, USA

- 30 12. Earth, Ocean and Atmospheric Sciences, Florida State University, Tallahassee, FL, USA
- 31 13. Faculty of Environmental Earth Science, Hokkaido University, Sapporo, Japan
- 32 14. NOAA/ESRL Global Monitoring Division, Boulder, CO, USA
- 33 15. Atmospheric Sciences Research Center, SUNY University at Albany, Albany, NY, USA
- 34 16. Finnish Meteorological Institute, Helsinki, Finland
- 35 17. The Institute of Meteorology and Water Management, National Research Institute, Warsaw,
- 36 Poland
- 37 18. Indonesian Institute of Aeronautics and Space (LAPAN), Bandung, Indonesia
- 38 19. Alfred Wegener Institute for Polar and Marine Research, Bremerhaven, Germany
- 39 20. Earth Observation Satellite Images Applications Lab (EOSIAL), Università di Roma 'La
- 40 Sapienza', Rome, Italy
- 41 21. Danish Meteorological Institute, Copenhagen, Denmark
- 42 22. Jet Propulsion Laboratory, California Institute of Technology, Pasadena, CA, USA
- 43 23. Department of Physics, New Mexico Institute of Mining and Technology, Socorro, NM,
- 44 USA
- 45 24. St. Edward's University, Austin, TX, USA
- 46 25. Department of Atmospheric Science, University of Alabama in Huntsville, Huntsville, AL,
- 47 USA
- 48 26. Department of Coupled Ocean-Atmosphere-Land Processes Research, Japan Agency for
- 49 Marine-Earth Science and Technology, Yokosuka, Japan
- 50 27. Global Environment and Marine Department, Japan Meteorological Agency, Tokyo, Japan
- 51 28. Université de la Réunion, Saint Denis, France
- 52 29. National Institute of Water and Atmospheric Research, Lauder, Central Otago, New Zealand
- 53 30. Universities Space Research Association, Greenbelt, MD, USA
- 54 31. Research Institute for Sustainable Humanosphere, Kyoto University, Kyoto, Japan
- 55 32. Upper Air and Surface Observation Department, Czech Hydrometeorological Institute,
- 56 Praha, Czech Republic
- 57 33. Air Quality Research Division, Environment & Climate Change Canada, Downsview, ON,
- 58 Canada.
- 59 34. Laboratoire d'Aerologie, Université de Toulouse, Toulouse, France

- 60 35. Observations & Infrastructure Division, Bureau of Meteorology, Melbourne, Victoria,
61 Australia
- 62 36. Earth Observing Laboratory, National Center for Atmospheric Research, Boulder, CO, USA
- 63 37. Alfred Wegener Institute, Potsdam, Germany
- 64 38. Science Systems and Applications Inc. Greenbelt, MD, USA
- 65 39. Atmospheric Research and Instrumentation Branch, National Institute for Aerospace
66 Technology (INTA), Madrid, Spain
- 67 *Correspondence to: Guanyu Huang (guanyu.huang@cfa.harvard.edu)

68 **Abstract**

69 We validate the Ozone Monitoring Instrument (OMI) ozone-profile (PROFOZ) product from
70 October 2004 through December 2014 retrieved by the Smithsonian Astrophysical Observatory
71 (SAO) algorithm against ozonesonde observations. We also evaluate the effects of OMI Row
72 anomaly (RA) on the retrieval by dividing the data set into before and after the occurrence of
73 serious OMI RA, i.e., pre-RA (2004-2008) and post-RA (2009-2014). The retrieval shows good
74 agreement with ozonesondes in the tropics and mid-latitudes and for pressure < ~50 hPa in the
75 high latitudes. It demonstrates clear improvement over the a priori down to the lower troposphere
76 in the tropics and down to an average of ~550 (300) hPa at middle (high latitudes). In the tropics
77 and mid-latitudes, the profile mean biases (MBs) are less than 6%, and the standard deviations
78 (SDs) range from 5-10% for pressure < ~50 hPa to less than 18% (27%) in the tropics (mid-
79 latitudes) for pressure > ~50 hPa after applying OMI averaging kernels to ozonesonde data. The
80 MBs of the stratospheric ozone column (SOC, the ozone column from the tropopause pressure to
81 the ozonesonde burst pressure) are within 2% with SDs of < 5% and the MBs of the tropospheric
82 ozone column (TOC) are within 6% with SDs of 15%. In the high latitudes, the profile MBs are
83 within 10% with SDs of 5-15% for pressure < ~50 hPa, but increase to 30% with SDs as great as
84 40% for pressure > ~50 hPa. The SOC MBs increase up to 3% with SDs as great as 6% and the
85 TOC SDs increase up to 30%. The comparison generally degrades at larger solar-zenith angles
86 (SZA) due to weaker signals and additional sources of error, leading to worse performance at
87 high latitudes and during the mid-latitude winter. Agreement also degrades with increasing
88 cloudiness for pressure > ~100 hPa and varies with cross-track position, especially with large
89 MBs and SDs at extreme off-nadir positions. In the tropics and mid-latitudes, the post-RA
90 comparison is considerably worse with larger SDs reaching 2% in the stratosphere and 8% in the
91 troposphere and up to 6% in TOC. There are systematic differences that vary with latitude
92 compared to the pre-RA comparison. The retrieval comparison demonstrates good long-term
93 stability during the pre-RA period, but exhibits a statistically significant trend of 0.14-0.7%/year
94 for pressure < ~ 80 hPa, 0.7 DU/year in SOC and -0.33 DU/year in TOC during the post-RA
95 period. The spatiotemporal variation of retrieval performance suggests the need to improve
96 OMI's radiometric calibration especially during the post-RA period to maintain the long-term
97 stability and reduce the latitude/season/SZA and cross-track dependence of retrieval quality.

98 **1 Introduction**

99 The Dutch-Finnish built Ozone Monitoring Instrument (OMI) on board the NASA Aura satellite
100 has been making useful measurements of trace gases including ozone and aerosols since October
101 2004. There are various retrieval algorithms to retrieve ozone profile and/or total ozone from
102 OMI data (Bak et al., 2015), including two independent operational total ozone algorithms
103 (Bhartia and Wellemeyer, 2002; Veefkind et al., 2006) and two ozone profile algorithms. Of the
104 two ozone profile algorithms, one is the operational algorithm (OMO3PR) developed at KNMI
105 (van Oss et al., 2001), and the other one is a research algorithm developed at Smithsonian
106 Astrophysical Observatory (SAO) by (Liu et al., 2010b). Both algorithms retrieve ozone profile
107 from the spectral region 270-330 nm using the optimal estimation method, but they differ
108 significantly in implementation details including radiometric calibration, radiative transfer model
109 simulation, a priori constraint, retrieval grids, and additional retrieval parameters. The SAO
110 ozone profile retrieval algorithm was initially developed for Global Ozone Monitoring
111 Experiment (GOME) data and was adapted to OMI data (Liu et al., 2010b). Total ozone column
112 (OC), Stratospheric Ozone Column (SOC) and Tropospheric Ozone Column (TOC) can be
113 directly derived from the retrieved ozone profile with retrieval errors in the range of a few
114 Dobson Units (DU) (Liu et al., 2006b; Liu et al., 2010a). This algorithm has been put into
115 production in the OMI Science Investigator-led Processing System (SIPS), processing the entire
116 OMI data record with approximately one-month delay. The ozone profile product titled
117 PROFOZ is publicly available at the Aura Validation Data Center (AVDC)
118 (<https://avdc.gsfc.nasa.gov/index.php?site=1389025893&id=74>). This long-term ozone profile
119 product, with high spatial resolution and daily global coverage, constitutes a useful dataset to
120 study the spatial and temporal distribution of ozone.

121 To effectively use the retrieval dataset, it is necessary to evaluate and understand its retrieval
122 quality and long-term performance. Although validation of the ozone profile product (mostly
123 earlier versions) has been partially performed against aircraft, ozonesonde, and Microwave Limb
124 Sounder (MLS) data, these evaluations are limited to certain time periods and/or spatial region
125 and/or to only portion of the product (e.g., total ozone columns (OC) or TOC only) (Bak et al.,
126 2013a; Hayashida et al., 2015; Lal et al., 2013; Liu et al., 2010a; Liu et al., 2010b; Pittman et al.,
127 2009; Sellitto et al., 2011; Wang et al., 2011; Yang et al., 2007; Ziemke et al., 2014).

128 Additionally, the quality of ozone profile retrievals is very sensitive to the signal to noise ratio
129 (SNR) of the radiance measurements as well as their radiometric calibration, which may degrade
130 over time as shown in GOME and GOME-2 retrievals (Cai et al., 2012; Liu et al., 2007).
131 Although OMI's optical degradation is remarkably small to within 1-2% over the years, the SNR
132 and the number of good spectral pixels (not flagged as bad/hot pixels) have been gradually
133 decreasing over the years due to the expected CCD degradation (Claas, 2014). Furthermore, the
134 occurrence of RA, which affects level 1b data at all wavelengths for particular viewing directions
135 or cross-track positions and likely due to blocking objects in the optical path, started in June
136 2007 affecting a few positions. This effect abruptly worsened in January 2009 affecting ~1/3 of
137 the cross-track positions (Kroon et al., 2011). The impacts of RA not only evolve with time but
138 also vary over the duration of an orbit. Analysis indicates that radiances in the UV1 channels
139 (shorter than ~310 nm) used in our retrievals might have been affected at all positions (Personal
140 communication with S. Marchenko) and are not adequately flagged for RA. Therefore, we need
141 to evaluate the impacts of instrument degradation and especially row anomaly on the temporal
142 performance of our ozone profile product. Currently, we are planning an update of the ozone
143 profile algorithm to maintain the long-term consistency of the product. The update will include
144 empirical correction of systematic errors caused by the instrument degradation and row anomaly
145 as a function of time. Such correction also requires us to evaluate the long-term retrieval quality
146 of our product.

147 To understand retrieval quality and the resulting spatial and temporal performance of our OMI
148 product, we evaluate our data from October 2004 through December 2014 against available
149 ozonesonde and MLS observations, respectively, in two papers. This paper evaluates our ozone
150 product including both ozone profiles and stratospheric and tropospheric ozone columns using
151 ozonesonde observations with a focus on retrieval quality in the troposphere. More than 27,000
152 ozonesonde profiles from both regular ozonesonde stations and field campaigns are used in this
153 study to provide a comprehensive and global assessment of the long-term quality of our OMI
154 ozone product. This paper is followed by the validation against collocated MLS data with a focus
155 on the retrieval quality in the stratosphere (Huang et al., 2017), also submitted to this special
156 issue).

157 This paper is organized as follows: Section 2 describes OMI retrievals and ozonesonde data. The
158 validation methodology is introduced in Section 3. Section 4 presents results, analysis and
159 discussions regarding the OMI and ozonesonde comparisons. Section 5 summarizes and
160 concludes this study.

161 **2 OMI and Ozonesonde Datasets**

162 **2.1 OMI and OMI Ozone Profile Retrievals**

163 OMI is a Dutch-Finnish built nadir-viewing pushbroom UV/visible instrument aboard the NASA
164 Earth Observing System (EOS) Aura satellite that was launched into a sun-synchronous orbit in
165 July 2004. It measures backscattered radiances in three channels covering the 270-500 nm
166 wavelength range (UV1: 270-310 nm, UV2: 310-365 nm, visible: 350-500 nm) at spectral
167 resolutions of 0.42-0.63 nm (Levelt et al., 2006). Measurements across the track are binned to
168 60 positions for UV2 and visible channels, 30 positions for the UV1 channels due to the weaker
169 signals. This results in daily global coverage with a nadir spatial resolution of 13 km \times 24 km
170 (along \times across track) for UV2 and visible channels, and 13 km \times 48 km for the UV1 channel.

171 The SAO OMI ozone profile algorithm was adapted from the GOME ozone profile algorithm
172 (Liu et al., 2005) to OMI and was initially described in detail in Liu et al. (2010b). Profiles of
173 partial ozone columns are retrieved at 24 layers, \sim 2.5 km for each layer, from the surface to \sim 60
174 km using OMI radiance spectra in the spectral region 270-330 nm with the optimal estimation
175 technique. In addition to the OC, SOC and TOC can be directly derived from the retrieved ozone
176 profile with the use of tropopause (defined based on the lapse rate) from the daily National
177 Center for Environmental Protection (NCEP) reanalysis data. The retrievals are constrained with
178 month- and latitude-dependent climatological a priori profiles derived from 15-year ozonesonde
179 and SAGE/MLS data (McPeters et al., 2007) with considerations of OMI random-noise errors.
180 OMI radiances are pre-calibrated based on two days of average radiance differences in the
181 tropics between OMI observations and simulations with zonal mean MLS data for pressure less
182 than 215 hPa and climatological ozone profile for pressure greater than 215 hPa. This “soft
183 calibration” varies with wavelength and cross-track positions but does not depend on space and
184 time.

185 The current algorithm of our SAO OMI ozone product that is used in this paper was briefly
186 described in Kim et al. (2013). The radiative transfer calculations have been improved through
187 the convolution of simulated radiance spectra at high resolutions rather than effective cross
188 sections, which is done by interpolation from calculation at selected wavelengths assisted by
189 weighting function. In addition, four spatial pixels along the track are coadded to speed up
190 production processes at a nadir spatial resolution of 52 km × 48 km. Meanwhile, minimum
191 measurement errors of 0.4% and 0.2% are imposed in the spectral ranges 270-300 nm and 300-
192 330 nm, respectively, to stabilize the retrievals. The use of floor errors typically reduces the
193 Degree of Freedom for Signals (DFS) and increases retrieval errors. Compared to the initial
194 retrievals, the average total, stratospheric, and tropospheric DFS decrease by 0.49, 0.27, and
195 0.22, respectively, and the mean retrieval errors in OC, SOC, and TOC increase by 0.6, 0.5, and
196 1.2 DU, respectively. The corresponding changes to the retrievals are generally within retrieval
197 uncertainties except for a systematic increase in tropospheric ozone at SZA larger than ~75°,
198 where the TOC increases to ~12 DU. Validation against ozonesonde data indicates that this TOC
199 increase at large SZA makes the retrieval worse. Therefore retrieved tropospheric ozone at such
200 large SZA should not be used, but the retrieved total ozone still shows good quality (Bak et al.,
201 2015).

202 For current products, retrievals contain ~5.5-7.4 DFS, with 4.6-7.3 in the stratosphere and 0-1.2
203 in the troposphere. Vertical resolution varies generally from 7–11 km in the stratosphere to 10–
204 14 km in the troposphere, when there is adequate retrieval sensitivity to the tropospheric ozone.
205 Retrieval random-noise errors (i.e., precisions) typically range from 0.6–2.5 % in the middle
206 stratosphere to approximately 12% in the lower stratosphere and troposphere. The solution
207 errors, dominated by smoothing errors, vary generally from 1-7% in the middle stratosphere to 7-
208 38% in the troposphere. The solution errors in the integrated OC, SOC, and TOC are typically in
209 the few DU range. Errors caused by the forward model and forward model parameter
210 assumptions are generally much smaller than the smoothing error (Liu et al., 2005). The main
211 sources of these errors include systematic errors in temperature and cloud-top pressure.
212 Systematic measurement errors are the most difficult to estimate, mostly due to lack of full
213 understanding of the OMI instrument calibration.

214 Certain cross track positions in OMI data have been affected by RA since June 2007 (Kroon et
215 al., 2011). Loose thermal insulating material in front of the instrument's entrance slit is believed
216 to block and scatter light, causing measurement error. The anomaly affects radiance
217 measurements at all wavelengths for specific cross-track viewing directions that are imaged to
218 CCD rows. Initially, the anomaly only affected a few rows. But since January 2009, the anomaly
219 has spread to other rows and shifted with time. The RA also shows slight differences among
220 different spectral channels, and varies during the duration of an orbit. Pixels affected by the RA
221 are flagged in the level 1b data. The science team suggested that they are not be used in research.
222 For data before 2009, the RA flagging is not applied in the processing. Pixels seriously affected
223 by RA will typically show enhanced fitting residuals. The algorithm was updated to use RA
224 flagging in the UV1 channel and was used to process the data starting from 2009. If a pixel is
225 flagged as a row anomaly then it is subsequently not retrieved to speed up the processing except
226 that the cross-track position 24 is still retrieved due to reasonably good fitting. It should be noted
227 that the retrieval quality of those non-flagged pixels may still be affected by the RA, because of
228 the different RA flagging in the UV1 and UV2, the lack of RA flagging before 2009 and
229 inadequacy of the RA flagging.

230 To screen out OMI profiles for validation, we only use OMI ozone profiles meeting the
231 following criteria based on three filtering parameters: 1) nearly clear-sky scenes with effective
232 cloud fraction less than 0.3; 2) cross track positions between 4 and 27, due to the relatively worse
233 quality and much larger footprint size of the off-nadir pixels beyond this range; 3) SZA should
234 be less than 75° due to very limited retrieval sensitivity to tropospheric ozone and the
235 aforementioned positive biases. The selection and justification of these criteria will be discussed
236 in Sects. 2.1.2-4.1.4, in which we will use all OMI pixels of each filtering parameter when
237 evaluating retrieval quality as a function of that specific parameter. The fitting quality of each
238 retrieval is shown in the fitting RMS (root mean square of the fitting residuals relative to the
239 assumed measurement errors). The mean fitting RMS including both UV1 and UV2 channels has
240 been increasing with time as shown in Figure 1. This is primarily due to the increase of fitting
241 residuals in UV1 caused by the instrument degradation and RA since the fitting residuals of UV2
242 only slightly increase with time. As aforementioned, the retrieval information of stratospheric
243 and tropospheric ozone mainly comes from UV1 and UV2, respectively. Consequently, retrievals

244 in the troposphere, the focus of this paper, are less impacted by the increasing fitting RMS.
245 However, to apply consistent filtering in validation against both ozonesonde in this study and
246 MLS data in the companion paper (Huang et al., 2017), we set the RMS threshold based on the
247 overall fitting RMS and select retrievals with fitting RMS smaller than the sum of monthly mean
248 RMS and its 2σ (i.e., Standard Deviations (SDs) of fitting RMS).

249 **2.2 Ozonesondes**

250 The balloon-borne ozonesonde is a well-established technique to observe the ozone profile from
251 the surface to ~ 35 km with vertical resolution of ~ 100 - 150 m and approximately 3-5% precision
252 and 5-10% accuracy (Deshler et al., 2008; Johnson, 2002; Komhyr, 1986; Komhyr et al., 1995;
253 Smit et al., 2007). Ozonesonde data have been widely used in the studies of stratospheric ozone,
254 climate change, tropospheric ozone and air quality, as well as the validation of satellite
255 observations (Huang et al., 2015; Kivi et al., 2007; Thompson et al., 2015; Wang et al., 2011).
256 However, the accuracy of ozonesonde observations depends on data processing technique, sensor
257 solution, and instrument type and other factors. Consequently, station-to-station biases may
258 occur in ozonesonde measurements and could be as great as 10% (Thompson et al., 2007c;
259 Worden et al., 2007).

260 A decade (2004-2014) of global ozonesonde data with locations shown in Figure 2, are utilized
261 in this study to validate our OMI ozone profile product. Most of our ozonesonde data were
262 obtained from the Aura Validation Data Center (AVDC) archive. It contains routine launches
263 from ozonesonde stations, mostly weekly and occasionally 2-3 times a week at some stations. It
264 also collects launches from field campaigns, for instance, IONS 06 (INTEX-B Ozone Network
265 Study 2006), ARCIONS (Arctic Intensive Ozonesonde Network Study)
266 (<http://croc.gsfc.nasa.gov/arcions/>) (Tarasick et al., 2010; Thompson et al., 2008). Data not
267 available at AVDC are obtained from other archives such as the World Ozone and Ultraviolet
268 Radiation Data Center (WOUDC) (<http://woudc.org/>), the Southern Hemisphere Additional
269 Ozonesondes (SHADOZ) (Thompson et al., 2007a; Thompson et al., 2007b), as well as archives
270 of recent field campaigns including DISCOVER-AQ (Deriving Information on Surface
271 Conditions from Column and Vertically Resolved Observations Relevant to Air Quality,
272 <http://discover-aq.larc.nasa.gov/>) (Thompson et al., 2015) and SEACR⁴S (Studies of Emissions

273 and Atmospheric Composition, Clouds and Climate Coupling by Regional Surveys,
274 <https://espo.nasa.gov/home/seac4rs>) (Toon et al., 2016). Almost all of the ozonesonde data in
275 this study were obtained from electrochemical concentration cell (ECC) ozonesondes, which is
276 based on the oxidation reaction of ozone with potassium iodide (KI) in solution. The exceptions
277 are Hohenpeissenberg station in Germany that uses Brewer-Mast (BM) ozonesondes, the New
278 Delhi, Poona, and Trivandrum stations that use Indian ozonesondes, and four Japanese stations
279 (i.e., Sapporo, Tsukuba, Naha and Syowa) that switched from KC ozonesondes to ECC
280 ozonesondes during late 2008 and early 2010. These types of ozonesondes have been reported to
281 have larger uncertainties than ECC ozonesondes (Hassler et al., 2014; Liu et al., 2013; WMO,
282 1998).

283 To avoid using anomalous profiles, we screen out ozonesondes that burst at pressure exceeding
284 200 hPa, ozone profiles with gaps greater than 3 km, more than 80 DU TOC or less than 100 DU
285 SOC. In the SOC comparison, we also filter measurements that do not reach 12 hPa. Some
286 ozonesonde data used in this paper (e.g. WOUDC data) are provided with a correction factor
287 (CF) derived by normalizing the integrated ozone column (appended with ozone climatology
288 above burst altitude) to the coincident total ozone column measured by a Dobson or Brewer
289 instrument to account for uncertainties mainly from the pump efficiency especially near the top
290 of the profiles. The CF is also included in our screening processes. If the CF is available, we
291 select ozonesonde profiles with the CF in the range of 0.85 to 1.15 to filter profiles that require
292 too much correction, and apply the correction. Finally, a small number of obviously erroneous
293 profiles are visually examined and rejected.

294 **3 Comparison Methodology**

295 Previous studies on the validation of satellite observations used a range of coincidence criteria.
296 Wang et al. (2011) set a 100 km radius and 3 hour time difference as coincidence criteria. Kroon
297 et al. (2011) applied coincidence criteria of $\pm 0.5^\circ$ for both latitude and longitude and 12 hours.
298 In this paper, we determine our coincident criteria based on the balance between finding most
299 coincident OMI/ozonesonde pairs to minimize differences due to spatiotemporal samplings and
300 finding a sufficient number of pairs for statistical analysis. For each screened ozonesonde profile,
301 we first select all filtered OMI data within $\pm 1^\circ$ latitude, $\pm 3^\circ$ longitude and ± 6 hours and then

302 find the nearest OMI retrieval within 100 km from the ozonesonde station to perform the
303 validation on the individual profile basis.

304 Ozonesondes have much finer vertical resolution than OMI retrievals. To account for the
305 different resolutions, ozonesonde profiles are first integrated into the corresponding OMI vertical
306 grids and then degraded to the OMI vertical resolution by using the OMI retrieval Averaging
307 Kernels (AKs) and *a priori* ozone profile based on the following equation:

$$308 \quad \hat{x} = x_a + A(x - x_a), \quad (1)$$

309 where x is the ozonesonde profile integrated into the OMI grid, \hat{x} is the retrieved ozone profile if
310 the ozonesonde is observed by OMI, A is the OMI AK matrix, and x_a is the OMI *a priori* ozone
311 profile. We refer to this retrieval as “convolved ozonesonde profile”, which is a reconstruction of
312 ozonesonde profile with OMI retrieval vertical resolution and sensitivity. Missing ozone profiles
313 above ozonesonde burst altitude are filled with OMI retrievals. The convolution process
314 essentially removes OMI smoothing errors and the impacts of *a priori* from the comparison so
315 that OMI/ozonesonde differences are mainly due to OMI/ozonesonde measurement precision,
316 spatiotemporal sampling differences and other errors. However, in the regions and altitudes
317 where OMI has low retrieval sensitivity, the comparisons can show good agreement because
318 both the retrieval and convolved ozonesonde approach the *a priori* profile. To overcome the
319 limitation of such a comparison, we also compare with unconvolved ozonesonde profiles since it
320 indicates how well the retrievals can represent the actual ozonesonde observations (i.e.,
321 smoothing errors are included as part of retrieval errors). In addition, we also compare OMI *a*
322 *priori* and convolved/unconvolved ozonesonde profiles to indicate the retrieval improvement
323 over the *a priori*.

324 For consistent calculations of TOC and SOC from the OMI/ozonesonde data, the tropopause
325 pressure included in the OMI retrieval and ozonesonde burst pressure (required to be less than 12
326 hPa or above ~30 km) are used as the proper boundaries. The TOC is integrated from the surface
327 to the tropopause. And the SOC is not the total stratospheric ozone column, but the ozone
328 column integrated from the tropopause pressure to the ozonesonde burst pressure.

329 The relative profile difference is calculated as (OMI- Sonde) / OMI *a priori* ×100% in the present
330 comparison with ozonesonde and with MLS in the companion paper. Choosing OMI *a priori*

331 rather than MLS/ozonesonde is to avoid unrealistic statistics skewed by extremely small values
332 in the reference data especially in the MLS retrievals of upper troposphere and lower
333 stratosphere ozone (Liu et al., 2010a). Unlike the profile comparison, ozonesonde/OMI
334 SOC/TOC values are used in the denominator in the computation of relative difference. To
335 exclude remaining extreme outliers in the comparison statistics, values that are exceeding 3σ
336 from the mean differences are filtered.

337 After applying the OMI/ozone filtering and coincident criteria, approximately 10,500
338 ozonesonde profiles are used in the validation. We performed the comparison for five latitude
339 bands: northern high latitudes (60° N- 90° N), northern mid-latitudes (30° N- 60° N), tropics (30°
340 S- 30° N), southern mid-latitudes (60° S- 30° S), and southern high latitudes (90° S- 60° S) to
341 understand the latitudinal variation of the retrieval performance. We investigated the seasonal
342 variations of the comparisons mainly at northern mid-latitudes where ozone retrieval shows
343 distinct seasonality and there are adequate coincidence pairs. To investigate the RA impacts on
344 OMI retrievals, we contrasted the comparison before (2004-2008, i.e., pre-RA) and after (2009-
345 2014, i.e., post-RA). Although we filter OMI data based on cloud fraction, cross-track position,
346 and SZA in the final evaluation of our retrievals against ozonesonde observations as shown in
347 Sect. 4.1.1., we conduct the comparison as a function of these parameters using coincidences at
348 all latitude bands to show how these parameters affect the retrieval quality as shown in the Sects.
349 4.1.2 – 4.1.4. In these evaluations, the filtering of OMI data based on cloud fraction, cross-track
350 position, and SZA are switched off, respectively. Approximately 15,000 additional ozonesonde
351 profiles are used in this extended evaluation. To evaluate the long-term performance of our
352 ozone profile retrievals, we analyze the monthly mean biases (MBs) of the OMI/ozonesonde
353 differences as a function of time using coincidences in the 60° S- 60° N region and then derive a
354 linear trends over the entire period as well as the pre-RA and post-RA periods.

355 **4 Results and Discussions**

356 **4.1 Comparison of Ozonesonde and OMI profiles**

357 **4.1.1 Ozone Profile Differences**

358 Comparisons of ozone profiles between OMI/a priori and ozonesondes with and without
359 applying OMI AKs for the 10-year period (2004-2014) are shown in the left panels of Figure 3.
360 The MBs and SDs vary spatially with altitude and latitude. Vertically, the SD typically
361 maximizes in the upper troposphere and lower stratosphere (UTLS) in all latitude bands due to
362 significant ozone variability and a priori uncertainty. Bak et al. (2013b) showed that the use of
363 Tropopause-Based (TB) ozone profile climatology with NCEP Global Forecast System (GFS)
364 daily tropopause pressure can significantly improve the a priori, and eventually reduce the
365 retrieval uncertainty. Consequently, the SDs of OMI/sonde differences in the UTLS at mid- and
366 high-latitudes can be reduced through reducing the retrieval uncertainties in a future version of
367 the algorithm that uses the TB climatology. Latitudinally, the agreement is better in the tropics
368 and becomes worse at higher latitudes. The patterns are generally similar in the northern and
369 southern hemispheres. The MBs between OMI and ozonesonde are within ~6% with AKs and
370 10% without AKs in the tropics and the middle latitudes. Large changes in the biases between
371 with and without AKs occur in the tropical troposphere where the bias differences reach 10%.
372 The MBs increase to 20-30% at high latitudes consistently with large oscillation from ~-20-30%
373 at ~300 hPa to +20% near the surface both with and without the application of AKs. At pressure
374 < 50 hPa, the SDs for comparisons with OMI AKs are typically 5-10% at all latitudes except for
375 the 90° S-60° S region. For pressure > 50 hPa, the SDs are within 18% and 27% in the tropics
376 and middle-latitudes, respectively, but increase to 40% at higher latitudes. The SDs for
377 comparison without applying OMI AKs, i.e., including OMI smoothing errors in the
378 OMI/ozonesonde differences, typically increase up to 5% for pressure < 50 hPa, but increase up
379 to 15-20% for pressure > ~50hPa. The smoothing errors derived from root square differences of
380 the MBs with and without OMI AKs are generally consistent with the retrieval estimate from the
381 optimal estimation.

382 The improvements of OMI over the climatological (a priori) profiles can be reflected in the
383 reduction of MBs and SDs in the comparisons between ozonesondes and OMI retrievals, and
384 between ozonesondes and a priori. The retrieval improvements in the MBs are clearly shown in
385 the tropics and at ~ 100 hPa pressure in the middle latitudes. At high latitudes, the MBs and
386 corresponding oscillations in the troposphere are much larger than these in the a priori
387 comparison, suggesting that these large biases are mainly caused by other systematic
388 measurements errors at high latitudes (larger SZAs and thus weaker signals). As can be seen
389 from the reduction of SDs, OMI retrievals show clear improvements over the a priori at pressure
390 < 300 hPa. For pressure > 300 hPa, the retrieval improvements vary with latitudes. There are
391 consistent retrieval improvements throughout the surface - 300hPa layer in the tropics and only
392 the 550 - 300 hPa layer at middle latitude, while there is no retrieval improvement over the a
393 priori for > 300 hPa at high latitudes. The failure to improve the retrieval over a priori in part of
394 the troposphere at middle and high latitudes is caused by several factors. They are the inherent
395 reduction in retrieval sensitivity to lower altitudes at larger SZAs as a result of reduced photon
396 penetration into the atmosphere, unrealized retrieval sensitivity arising from retrieval
397 interferences with other parameters (e.g., surface albedo) as discussed in Liu et al. (2010b) and
398 the use of floor-noise of 0.2% that underestimates the actual OMI measurement SNR. In
399 addition, the a priori ozone error in the climatology is quite small since the SDs of the
400 differences between the a priori and ozonesonde without AKs are typically less than 20% in the
401 lower troposphere for middle and high latitudes, which also makes it more difficult to improve
402 over the a priori comparison.

403 The right column of Figure 3 shows the comparisons between OMI retrievals and ozonesondes
404 convolved with OMI AKs in the pre-RA and post-RA periods, respectively. In the tropics and
405 mid-latitudes, the pre-RA comparison is better than the post-RA comparison, with SDs smaller
406 by up to $\sim 8\%$ at most altitudes especially in the troposphere. The pre-RA comparison also shows
407 smaller biases near ~ 300 hPa at middle latitudes while the post-RA comparison exhibits negative
408 biases reaching 8-12%. At high latitudes, the pre-RA period does not show persistent
409 improvement during the post-RA period. The pre-RA comparison shows slightly smaller SDs at
410 most altitudes and smaller negative biases by 10% around 300 hPa in the northern high latitudes,
411 and smaller positive biases by 20% near the surface in the southern high latitudes. The worse

412 results during the post-RA period are caused by increasingly noisy OMI measurements with
413 smaller SNR and the additional radiometric biases made by the RA, which vary with space and
414 time. The smaller SDs at some altitudes of high latitudes may reflect a combination of ozone
415 variation, uneven distribution of ozonesondes with varying uncertainty at different stations, and
416 cancellation of radiometric errors by the RA.

417 As seen from the number of OMI/ozonesonde coincidences shown in Figure 3, the northern mid-
418 latitudes and the tropics have sufficient coincidences to validate the retrievals as a function of
419 season. In the tropics, the retrieval comparison does exhibit little seasonality as expected (not
420 shown). Figure 4 shows the comparison similar to Figure 3(c) for each individual season at
421 northern middle latitudes. The comparison results are clearly season-dependent with different
422 altitude-dependent bias patterns, and with the smallest SDs in the summer (except for the MBs)
423 and the worst SDs in the winter. This indicates the general best retrieval sensitivity to lower
424 tropospheric ozone during the summer as a result of small SZAs and stronger signals and worst
425 retrieval sensitivity during the winter as a result of large SZAs and weaker signals. The MBs for
426 with and without AKs at 300 hPa vary from ~12% in the winter to -10% in the summer. The
427 overall MBs are the smallest during the spring, within 6%; but the MBs at pressure < 50 hPa are
428 the best during the summer. The maximum SDs vary from 31% in the winter to 20% in the
429 summer. Also, the retrieval in the summer shows the most improvements in terms of reduction in
430 SDs over the a priori in the lower troposphere at all tropospheric layers except for the bottom
431 layer, while the retrievals during other seasons show the improvement over a priori only above
432 the lowermost two/three layers. The seasonal variation of retrieval quality is partially caused by
433 the seasonal variations of the retrieval sensitivity and ozone variability. Bak et al. (2013b)
434 showed that the use of TB ozone climatology with daily NCEP GFS tropopause pressure can
435 significantly reduce the seasonal dependence of the comparison with ozonesondes. In addition,
436 radiometric calibration errors such as those caused by stray light and RA also contribute to the
437 seasonal variation of retrieval quality.

438 **4.1.2 Solar Zenith Angle Dependence**

439 The SZA of low earth orbit (LEO) satellite observation varies latitudinally and seasonally;
440 therefore the SZA dependence of the retrieval can cause latitudinal and seasonal dependent

441 retrieval biases. SZA is one of the main drivers that affect retrieval sensitivity especially to
442 tropospheric ozone. At large SZA, the measured backscattered signal becomes weak due to weak
443 incoming signal and long path length; the retrieval sensitivity to the tropospheric ozone
444 decreases due to reduced photon penetration to the troposphere. In addition, measurements are
445 subject to relatively larger radiometric errors such as those from stray light and as a result of
446 weaker signal, and radiative transfer calculations can lose accuracy at larger SZA (Caudill et al.,
447 1997).

448 Figure 5 gives the MBs and SDs of differences between OMI and ozonesondes (with OMI AKs)
449 in a function of SZAs. We can see that retrieval performance generally becomes worse at large
450 SZA. The SD typically increases with SZA especially at pressure > 300 hPa. At SZA larger than
451 75°, the SD at ~300 hPa increases to greater than ~45%. The variation of MBs with SZA is more
452 complicated. We see generally larger positive biases at larger SZA in the troposphere with >
453 20% biases at SZA larger than 75°. The MBs near ~ 30 hPa becomes more negative at larger
454 SZAs. There is a strip of positive biases of ~10% that slightly decreases in pressure from ~50
455 hPa at low SZA to ~10 hPa at large SZA; it might be due to some systematic radiometric biases
456 that can affect ozone at different altitudes varying with SZA. Because of the clear degradation of
457 the retrieval quality at large SZA, we set the SZA filtering threshold of 75° to filter OMI data.

458 **4.1.3 Cloud Fraction Dependence**

459 The presence of cloud affects retrieval sensitivity since clouds typically reduce sensitivity to
460 ozone below clouds and increase sensitivity to ozone above clouds. The accuracy of ozone
461 retrievals is sensitive to the uncertainties of cloud information and cloud treatment (Antón and
462 Loyola, 2011; Bak et al., 2015; Liu et al., 2010a). Our OMI ozone algorithm assumes clouds as
463 Lambertian surfaces with optical centroid cloud pressure from the OMI Raman cloud product
464 (Vasilkov et al., 2008), and partial clouds are modeled using independent pixel approximation
465 such that the overall radiance is the sum of clear and cloudy radiances weighted by the effective
466 cloud fraction. The cloud albedo is assumed to be 80% and is allowed to vary (>80%) with the
467 effective cloud fraction.

468 Figure 6 gives the influences of effective cloud fraction on the comparisons between OMI and
469 ozonesonde observations convolved with OMI AKs. The MBs and SDs do not change much with

470 cloud fraction for pressure < 100 hPa, and typically increase with the increase of cloud fraction
471 for pressure > 100 hPa. The MBs at pressure > 100 hPa, especially greater~300 hPa, increase to
472 more than 10% with cloud fraction greater than ~0.3. This indicates that the cloud fractions have
473 small impacts on the stratospheric retrievals but large impacts on the tropospheric retrievals as
474 expected. Some of the variation with cloud fraction such as negative biases near ~300 hPa at
475 cloud fraction of ~0.4 and the decreases of positive biases at ~ 50 hPa for cloud fraction greater
476 than ~0.8 may be partially related to the uncertainties of the cloud parameters. The chosen
477 filtering threshold of 0.3 in cloud fraction is a tradeoff between validating OMI data with
478 adequate retrieval sensitivity to tropospheric ozone and finding adequate number of
479 OMI/ozonesonde coincidences.

480 **4.1.4 Cross-Track Position Dependence**

481 The OMI swath is divided into 30 cross-track pixels at the UV1 spatial resolution of our product.
482 Each cross-track position is measured by a different part of the CCD detector, i.e., essentially a
483 different instrument. Radiometric calibration coefficients of the instrument are characterized
484 during pre-launch only at selected CCD column pixels and then interpolated to other columns,
485 causing variation in the radiometric calibration performance across the CCD detector. This in
486 turn causes cross-track dependent biases in the calibrated radiance (Liu et al., 2010b), which
487 therefore causes striping in almost all the OMI data products if no de-striping procedure is
488 applied. Our retrieval algorithm has included a first-order empirical correction independent of
489 space and time to remove the cross-track variability (Liu et al., 2010b). However, residual
490 dependence on cross-track position remains and the radiometric calibration at different position
491 can degrade differently with time (e.g., the RA impact). In addition, the viewing zenith angle
492 ranges from ~0° to ~70° and the footprint area increases by approximately an order of magnitude
493 from nadir to the first/last position. So the varying viewing zenith angle causes the variation of
494 retrieval sensitivities and atmospheric variabilities within varying footprint areas may also cause
495 additional cross-track dependence in the retrieval performance.

496 Figure 7 provides the MBs and SDs of the differences between OMI and ozonesonde convolved
497 with OMI AKs as a function of cross-track position for pre-RA and post-RA periods,
498 respectively. It clearly exhibits cross-track dependence especially with large positive/negative

499 MBs and large SDs at the first/last several extreme off-nadir positions. This is why we select
500 cross-track positions of 4-27 in the validation to avoid positions with large biases. The enhanced
501 biases/SDs at positions 24 (RA flagging not applied) and 27 (flagged as RA in UV2 since June
502 25, 2007 but not flagged/applied in UV1) are due to the RA impact during the post-RA period.
503 Cross-track positions 1-10 show consistent bias patterns with negative biases in ~300- 50 hPa
504 layer and positive biases in ~surface – 300 hPa layer, and large standard deviation around ~ 300
505 hPa although the magnitude decreases with increasing cross-track position. This pattern occurs
506 during both pre-RA and post-RA periods although the values are larger during the post-RA
507 period. For other cross-track positions, the variation is relatively smaller but we can still see
508 small striping patterns.

509 **4.2 Comparison of Partial Ozone Columns**

510 We investigate and validate OMI partial ozone columns, including SOCs, TOCs, and surface-
511 550 hPa and surface-750 hPa ozone columns in this section. We define the lowermost one and
512 two layer as surface-750 hPa and surface-550 hPa in this paper, respectively, for conveniences.
513 Similarly, we also analyze the validation results of SOCs and TOCs during pre-RA and post-RA,
514 respectively, to test the impacts of RA on OMI partial ozone columns. In addition, we validate
515 ozone columns from the surface to ~550 hPa (bottom two layers) and ~ 750 hPa (bottom one
516 layer) against ozonesonde observations in the tropics and mid-latitude summer where there is
517 better retrieval sensitivity to these quantities.

518 **4.2.1 Comparison of Stratospheric Ozone Columns (SOCs)**

519 The left column of Figure 8 shows the MBs and SDs of the comparisons of OMI and ozonesonde
520 SOCs for each of the five latitude bands during 2004-2014. In all regions, the OMI SOCs have
521 excellent agreement with ozonesonde SOCs regardless of whether ozonesonde data are
522 convolved with OMI AKs. The application of OMI AKs to ozonesonde SOCs only slightly
523 improves the comparison statistics. The MBs with OMI AKs are within 1.8% except for a
524 negative bias of 3% at northern high latitudes, while the SDs are within 5.1% except for 5.7% at
525 high latitudes. The correlation coefficient is greater than 0.95 except for 0.90 in the tropics due to
526 the smaller SOC range. The SDs are typically larger than the comparisons with MLS data (Liu et

527 al., 2010a) due to worse coincidence criteria, relatively larger uncertainty in the ozonesonde
528 stratospheric ozone columns compared to MLS data, and different altitude ranges of integration.

529 The middle and right columns of Figure 8 show comparison results during the pre-RA and post-
530 RA periods, respectively. The comparison is typically better during the pre-RA with SDs smaller
531 by 0.2-0.6% and larger correlation coefficients although the MBs are generally smaller during
532 the post-RA period. One exception is at southern high-latitudes where the post-RA comparison
533 statistics are significantly better except for the MB, consistent with Figure 3, likely due to a
534 combination of ozone variation between these two periods, uneven distribution of ozonesondes
535 at different stations, and cancellation of various calibration errors.

536 **4.2.2 Comparison of Partial Ozone Columns in the Troposphere**

537 The left column of Figure 9 shows the comparison of OMI and ozonesonde (with and without
538 OMI AKs) TOCs for each of the five latitude bands during 2004-2014. Without applying OMI
539 AKs, the MBs are within 1-3% except for 9% at northern high latitudes; The SDs are within 20%
540 in the tropics and mid-latitudes and increase to ~30-40% at high-latitudes. The correlation
541 coefficient ranges from 0.83 in the tropics to ~0.7 at middle latitudes, and 0.5-0.6 at high-
542 latitudes. The linear regression slopes are in the range 0.6-0.8 typically smaller at high latitudes
543 due to reduced retrieval sensitivity to the lower troposphere. After applying the OMI AKs to
544 ozonesonde data to remove smoothing errors, we see significant improvement in the comparison
545 statistics except for MBs, which are within 6% at all latitudes. The SDs are reduced to within
546 15% in the tropics and middle latitudes and ~30% (5.5-8.1 DU) at high latitudes; the correlation
547 improves by 0.04-0.12 and the slope significantly increases by 0.12-0.23 to the range 0.8-1.0 at
548 different latitude bands due to accounting for inadequate retrieval sensitivity to the lower and
549 middle troposphere.

550 The middle and right columns of Figure 9 show comparisons during pre-RA and post-RA,
551 respectively. The comparison between OMI and ozonesondes with OMI AKs TOCs during the
552 pre-RA period is significantly better than these during the post-RA period in the tropics and mid-
553 latitudes with SDs smaller by 3.4-5.5% and greater correlation. The MBs during the post-RA
554 period is smaller by ~2 DU at mid-latitudes, but larger by ~1 DU in the tropics. However, the

555 post-RA comparison is similar to the pre-RA comparison at northern high-latitudes and is even
556 better at southern high latitudes probably due to the aforementioned ozonesonde issues.

557 Figure 10 shows examples of time series when comparing individual OMI and ozonesondes
558 (with OMI AKs) TOCs and their corresponding differences at six selected stations, one for each
559 latitude region of 90° N-60° N, 60° N-30° N, 30° N-0°, 0°-30° S, 30° S-60° S and 60° S-90° S.
560 OMI TOC shows good agreement with ozonesondes at these stations with overall MBs ≤ 3 DU
561 and SDs less than 5.1 DU. The comparison is also good even in the high latitude regions partially
562 because the Summit and Neymayer stations only have ozonesonde launches during local
563 summer. Seasonal dependent biases are clearly seen at Payerne, and bias trends can be seen at
564 several stations with positive trends at Summit and Neumayer and a negative trend at Naha. In
565 the pre-RA and post-RA periods, the MBs are typically within 2 DU and the SDs are typically
566 smaller during the pre-RA period except for Naha. The better comparison (both mean bias and
567 standard deviation) during the post-RA period at Naha is likely due to the switch to ECC
568 ozonesondes beginning on November 13, 2008 from KC ozonesonde that have greater
569 uncertainty (WMO, 1998).

570 Figure 2 also shows the MBs and SDs of the TOC differences between OMI and ozonesonde
571 convolved with OMI AKs at each station/location where there are at least 10 coincident
572 OMI/ozonesonde pairs. OMI data generally exhibit good agreement with ozonesondes at most of
573 the stations, with MBs of ≤ 3 DU and SDs of ≤ 6 DU. In the tropics (30° S-30° N), very large
574 SDs (>11 DU) occur at the two Indian stations (New Delhi, and Trivandrum). In addition, there
575 is a large bias of > 6 DU at New Delhi. The poor comparisons at these two stations are likely
576 associated with the large uncertainties of the Indian ozonesonde data. Hilo has large biases of
577 ~ 4.5 DU with 3.2 and 6.2 DU for pre-RA and post-RA, respectively. Java also has a large bias of
578 ~ 5 DU but shows little difference between pre-RA and post-RA. Consistent $\sim 2\%$ and $\sim 5\%$
579 underestimates of OC by ozonesondes compared to OMI total ozone are found in Hilo and Java,
580 respectively (Thompson et al., 2012). These OC underestimates may partly explain the large
581 TOC biases in Hilo and Java. However, the reason for underestimates of ozonesonde-derived OC
582 is unknown. In the middle latitudes, noticeably large SDs and/or biases occur at a few stations
583 such as Churchill, Sable Islands, Hohenpeissenberg, and Parah. Three Japanese stations,
584 Sapporo, Tateno, and Naha, exhibit relatively large biases of 2-3 DU and even larger biases

585 before switching from KC to ECC sondes. Almost half of the 11 northern high latitude stations
586 (60° N- 90° N) and two of the 6 southern high-latitude stations have large SDs/biases. In addition
587 to retrieval biases from the OMI data, some of the large biases or SDs might be partially related
588 to ozonesonde type with different biases and uncertainties due to different types (e.g., Indian
589 sonde stations, Brewer-Mast ozonesonde at Hohenpeissenberg, three KC sonde stations),
590 manufacturers (e.g., SP vs. ENSCI for ECC sonde), sensor solution or related to individual sonde
591 operations, which was shown in the validation of GOME ozone profile retrievals (Liu et al.,
592 2006a).

593 Figure 11 shows the comparison for each season at northern mid-latitudes. Consistent with
594 profile comparison, the TOC comparison is season-dependent. When applying OMI AKs, the
595 mean bias varies from 3 DU in winter to -1.5 DU in summer. The SDs are within 6.8 DU with
596 the smallest value during fall due to less ozone variability. The regression slopes are very close,
597 within 0.04 around 0.67. The retrieval sensitivity is smallest during the summer as seen from the
598 greatest correlation and slope and relatively small standard deviation, and is the worst during the
599 winter. With OMI AKs applied to ozonesonde profiles, the MBs only slightly change (varying
600 from 3.5 DU to -1.3 DU), but the SDs are significantly reduced to within 5.2 DU, the slopes
601 significantly increase by ~ 0.2 to 0.8-1.0, and the correlation improves significantly during the
602 winter and spring.

603 Figure 12 compares the surface \sim 550 hPa and surface \sim 750 hPa ozone columns with ozonesonde
604 data in the middle latitudes during summer and the tropics. Compared to the TOC comparisons
605 in Figure 9 and Figure 11, the comparisons of these lower tropospheric ozone columns exhibit
606 smaller regression slopes and correlations that are a result of reduced retrieval sensitivity. In the
607 tropics, the slopes decrease from 0.78 in TOC to 0.65 in the surface \sim 550 hPa ozone column and
608 ~ 0.50 in the surface \sim 750 hPa column, with corresponding correlation from 0.83 to 0.74 in the
609 surface \sim 550 hPa column, and 0.66 in the surface \sim 750 hPa column. This indicates that the
610 retrievals in the surface \sim 550 hPa/750 hPa can capture $\sim 65\%/50\%$ of the actual ozone change
611 from the a priori. During the middle latitude summer, the slope decreases from 0.71 in the TOC
612 comparisons to 0.42 in the surface \sim 550 hPa comparisons and 0.32 in the surface \sim 750 hPa
613 comparisons, with corresponding correlation coefficients from 0.74 to 0.5 and 0.46. Thus, the
614 retrievals in the surface \sim 550 hPa and \sim 750 hPa only capture $\sim 40\%/30\%$ of the actual ozone

615 change from the a priori. The MBs are generally small within 0.5 DU (5%) with SDs of ~3.6 DU
616 (20-28%) in the surface~550 hPa ozone column and ~2.5 DU (25-36%) in the surface~750 hPa
617 ozone column. After applying OMI AKs to account for inadequate retrieval sensitivity and
618 removing smoothing errors, the slope significantly increases to approach 1 (as expected). SDs
619 are reduced to ~10% in the middle latitudes and ~15% in the tropics.

620 **4.3 Evaluation of Long-term Performance**

621 Comparisons in Sects 4.1 and 4.2 indicated systematic differences between pre-RA and post-RA
622 periods and generally worse performance during the post-RA periods. To further illustrate the
623 long-term stability of our ozone profile product and understand the quality of OMI radiometric
624 calibration as a function of time, we analyze monthly MBs of OMI/ozonesonde differences with
625 OMI retrieval AKs in ozone profiles, SOCs, and TOCs. Due to the lack of OMI observations
626 during some months at high-latitudes, we focus the evaluation by using coincidence pairs in 60°
627 S-60° N. Monthly MBs are calculated only if there are more than 5 OMI-ozonesonde pairs in a
628 given month. Linear regression trend is on the MBs for the entire period (2004-2014) and/or for
629 the pre-RA and post-RA periods, respectively. The trend is considered statistically significant if
630 its P value is less than 0.05.

631 The linear trends of monthly mean ozone biases for each OMI layer between 60° S-60° N are
632 plotted in Figure 13 for each of the three periods. During 2004-2014, marked in black, ozone
633 biases at layers above 50.25 hPa show significant positive trends of 0.06-0.17 DU/year (0.17-
634 0.52%/year), while ozone biases between 290 hPa and 110 hPa exhibit significant negative
635 trends of 0.1-0.19 DU/year (1-2%/year). The positive trends in the stratosphere are generally
636 consistent with those shown in OMI-MLS comparisons (Huang et al., 2017). In the lowermost
637 three OMI layers, ozone differences are more stable but with several large spikes during the post-
638 RA periods likely due to the RA evolution or instrument operation. The derived trends for the
639 pre-RA period are generally more flat and insignificant at all layers indicating good stability of
640 our product as well as the OMI radiometric calibration. During the post-RA period, the derived
641 trends are positive above 75 hPa with statistical significance. These positive trends in the
642 stratosphere are generally similar to those over the entire period, suggesting the dominant
643 contribution of the post-RA period to the overall trend. In the altitude range 214 – 108 hPa, the

644 post-RA trends are also flat similar to the pre-RA trends, but the values are systematically
645 smaller during the post-RA period, causing significantly negative trends over the entire period.

646 The SOC biases exhibit small positive trend of 0.14 ± 0.09 DU/year in 2004-2014 with no
647 statistical significance (Figure 14(a)). This slight positive trend is a result of trend cancellation
648 by the positive trends above 80 hPa and negative trends between 220 hPa and 80 hPa The TOC
649 biases reveal a significant negative trend of -0.18 ± 0.05 DU/year (Figure 14(b)), mostly from
650 layers in the upper troposphere. In the pre-RA and post-RA periods, both trends of both SOC and
651 TOC biases are relatively flat during the pre-RA period, while the SOC trend in the post-RA
652 period is 0.77 ± 0.20 DU/year with significance. It is noticeable that the P value of TOC trend in
653 the post-RA period is 0.06.

654 The significant trends of ozone biases at different layers as well as in SOC and TOC suggest that
655 the current ozone profile product is not suitable for trend studies especially during the post-RA
656 period. The relatively flat bias trends during the pre-RA periods and statistically significant
657 trends during the post-RA period confirm that the better stability of our product during the pre-
658 RA period and more temporal variation of the retrieval performance during the post-RA period
659 are likely associated with the RA evolution. In previous sections, the validation of our retrievals
660 revealed latitudinal/seasonal/SZA and cross-track dependent biases even during the pre-RA
661 period. This indicates the need to remove signal dependent errors and the calibration
662 inconsistency across the track. To maintain the spatial consistency and long-term stability of our
663 ozone profile product, we need to further improve OMI's radiometric calibration especially
664 during the post-RA period. Preferably, the calibration improvement should be done in the level
665 0-1b processing. If this option is not possible, we can perform soft calibration similar to Liu et al.
666 (2010b) but derive the correction as a function of time and latitude/SZA. In addition, it should be
667 noted that the trend calculation might be affected by factors such as the availability of correction
668 factors with ozonesondes (Morris et al., 2013), station-to-station variability and the uneven
669 spatiotemporal distribution of the ozonesondes, which can introduce considerable sampling
670 biases (Liu et al., 2009; Saunois et al., 2012).

671 **5 Summary and Conclusion**

672 We conducted a comprehensive evaluation of the quality of OMI ozone profile (PROFOZ)
673 products produced by the SAO algorithm, including their spatial consistency and long-term
674 performance using coincident global ozonesonde observations during the decade 2004-2014. To
675 better understand retrieval errors and sensitivity, we compared the retrieved ozone profiles and a
676 priori profile at individual layers with ozonesondes before and after being degraded to the OMI
677 vertical resolution with OMI retrieval average kernels (AKs). We also compared the integrated
678 SOC, TOC, and surface-~550/~750 hPa ozone columns with ozonesonde data. To understand the
679 spatial distribution of retrieval performance, the validations are grouped into five latitude ranges:
680 northern/southern high/middle latitudes, and the tropics. To investigate the impacts of the OMI
681 row anomaly (RA) on the retrievals, we contrasted the comparison before and after the
682 occurrence of major OMI RA in January 2009, i.e., pre-RA (2004-2008) and post-RA (2009-
683 2014) periods. In addition, we quantified the dependence of retrieval performance on seasonality
684 and several key parameters including solar zenith angle (SZA), cloud fraction, and cross-track
685 position. Finally, we analyzed the monthly mean variation of the mean biases (MBs) to examine
686 the long-term stability of the PROFOZ product.

687 The comparison between OMI and ozonesonde profiles varies in altitude, with maximum
688 standard deviations (SDs) in the Upper Troposphere and Lower Stratosphere (UTLS) due to
689 significant ozone variability, and varies with latitude similarly in the northern and southern
690 hemispheres. There is good agreement throughout the atmosphere in the tropics and mid-
691 latitudes. With the application of OMI AKs to ozonesonde data, the MBs are within 6%, and the
692 SDs increase from 5-10% for pressure < ~50 hPa to within 18%(27%) in the tropics/mid-
693 latitudes for pressure > ~50 hPa. In the high latitudes, the retrievals agree well with ozonesondes
694 only for pressure < ~50 hPa with MBs of < 10% and SDs of 5-15% for pressure < ~ 50 hPa, but
695 with MBs reaching 30% and SDs reaching 40% for pressure > ~50 hPa. The comparison results
696 are seasonally dependent. At northern mid-latitudes, there are generally the best retrieval
697 sensitivity and the smallest SDs as great as 20% in the summer, and the worst sensitivity and the
698 largest SDs reaching 31% in the winter. The MBs near 300 hPa vary from 12% in the winter to -
699 10% in the summer. The post-RA comparison is generally worse in the tropics and mid-latitudes
700 than the pre-RA comparison, with SDs larger by up to 8% in the troposphere and 2% in the

701 stratosphere, and with larger MBs around ~300 hPa in the mid-latitudes. But at high latitudes, the
702 pre-RA comparison does not show persistent improvement over the post-RA comparison, with
703 smaller biases and larger SDs at some altitudes, especially at southern high latitudes. The
704 retrieval improvement over a priori can be determined from the SD reduction of the retrieval
705 comparison from the a priori comparison. The retrievals demonstrate clear improvement over the
706 a priori down to the surface in the tropics, but only down to ~750 hPa during mid-latitude
707 summer, ~550 hPa during the other seasons of mid-latitudes and ~ 300 hPa at high latitudes.

708 Retrieval performance typically becomes worse at large SZA, especially at SZA larger than 75°,
709 where the MBs in the troposphere are >20% and the SDs near ~300 hPa are > 45%. The worse
710 performance at larger SZA is due to a combination of weaker signal and greater influence by
711 radiometric calibration errors such as due to stray light, and radiative transfer calculation errors.
712 The variation of SZA is likely responsible for the majority of the retrieval dependence on latitude
713 and season. The retrieval quality for pressure > ~100 hPa degrades with increasing cloudiness in
714 terms of MBs and SDs, with MBs greater than 10% at cloud fraction > 0.3. The retrieval
715 performance also varies with cross-track position, especially with large MBs and SDs at the
716 first/last extreme off-nadir positions (e.g., 1-3 and 28-30). The dependence is stronger during the
717 post-RA period.

718 The integrated SOCs and TOCs also exhibit good agreement with ozonesondes. With the
719 convolution of OMI AKs to ozonesonde data, the SOC MBs are within 2% with SDs within
720 ~5.1% in the tropics and mid-latitudes. These statistics do not change much even without the
721 applications of OMI AKs. The comparison becomes slightly worse at high latitudes, with MBs
722 up to 3% and SDs up to 6%. The pre-RA comparison is generally better with smaller SDs of 0.2-
723 0.6% except for southern high latitudes, although with slightly larger MBs. The TOC MBs and
724 SDs with OMI AKs are within 6%, with SDs of <~15% in the tropics and mid-latitudes but reach
725 30% at high latitudes. The pre-RA TOC comparison is also better in the tropics and mid-latitudes
726 with SDs smaller by 3.4-5.5% but worse values at southern high latitudes. The TOC comparison
727 at northern mid-latitudes varies with season, with MBs of 11%. There are worse correlation
728 during winter and MBs of -3% and best correlation in summer. The TOC comparison also shows
729 noticeable station-to-station variability in similar latitude ranges with much larger MBs and/or
730 SDs at the two Indian stations and larger MBs at several Japanese stations before they switched

731 from KC ozonesondes to ECC ozonesondes. This demonstrates the impacts of ozonesonde
732 uncertainties due to sonde types, manufacturers, sensor solution and operations. Without
733 applying OMI AKs, the TOC correlation with ozonesondes typically becomes worse at higher
734 latitudes, ranging from 0.83 in the tropics to 0.5-0.6 at high latitudes. The linear regression slope
735 is within 0.6-0.8, typically smaller at higher latitudes, reflecting the smaller retrieval sensitivity
736 down to the troposphere at higher latitudes mainly resulting from larger SZA. The convolution of
737 AKs significantly improves the correlation and slope. The impact of retrieval sensitivity related
738 to SZA is also reflected in the seasonal dependence of the comparison at mid-latitudes.

739 The surface-~550/750 hPa ozone columns in the tropics during mid-latitude summer compare
740 quite well with ozonesonde data, with MBs of < 5% and SDs of 20-25%/28-36% without OMI
741 AKs. The correlation and slope decrease with decreasing altitude range due to reduced retrieval
742 sensitivity down to the lower troposphere. These columns capture ~65%/50% of the actual ozone
743 change in the tropics and ~40%/30% in the troposphere. Convoluting ozonesonde data with OMI
744 AKs significantly increases the slope to ~1 and reduce the SDs to 10-15%.

745 The contrast of pre-RA and post-RA comparisons indicates generally worse post-RA
746 performance with larger SDs. Linear trend analysis of the OMI/ozonesonde monthly MBs further
747 reveals additional RA impact. The temporal performance over 60° S-60° N is generally stable
748 with no statistically significant trend during the pre-RA period, but displays a statistically
749 significant trend of 0.14-0.7%/year at individual layers for pressure < ~80 hPa, 0.7 DU/year in
750 SOC and -0.33 DU/year in TOC during the post-RA period. Because of these artificial trends in
751 our product, we caution against using our product for ozone trend studies.

752 This validation study demonstrates generally good retrieval performance of our ozone profile
753 product especially in the tropics and mid-latitudes during the pre-RA period. However, the
754 spatiotemporal variation of retrieval performance suggests that OMI's radiometric calibration
755 should be improved, especially during the post-RA period, including the removal of signal-
756 dependent errors, calibration inconsistency across the track and with time to maintain the long-
757 term stability and spatial consistency of our ozone profile product.

758 **Data Availability**

759 OMI PROFOZ (version 0.9.3) used in this study is available to users at Aura Validation Data
760 Center (AVDC) (<https://avdc.gsfc.nasa.gov/index.php?site=1389025893&id=74>).

761 **Acknowledgements**

762 This study was supported by the NASA Atmospheric Composition: Aura Science Team
763 (NNX14AF16G) and the Smithsonian Institution. The Dutch-Finnish OMI instrument is part of
764 the NASA EOS Aura satellite payload. The OMI Project is managed by NIVR and KNMI in the
765 Netherlands. We acknowledge the OMI International Science Team for producing OMI data. We
766 also acknowledge the ozonesonde providers and their funding agencies for making ozonesonde
767 measurements, and the Aura Validation Data Center (AVDC), WOUDC, SHADOZ,
768 DISCOVER-AQ, and SEACR⁴S for archiving the ozonesonde data.

769 **References**

- 770 Antón, M., and Loyola, D.: Influence of cloud properties on satellite total ozone observations, *J.*
771 *Geophys. Res.*, 116, doi: 10.1029/2010JD014780, 2011.
- 772 Bak, J., Kim, J. H., Liu, X., Chance, K., and Kim, J.: Evaluation of ozone profile and
773 tropospheric ozone retrievals from GEMS and OMI spectra, *Atmos. Meas. Tech.*, 6, 239-249,
774 2013a.
- 775 Bak, J., Liu, X., Kim, J. H., Chance, K., and Haffner, D. P.: Validation of OMI total ozone
776 retrievals from the SAO ozone profile algorithm and three operational algorithms with Brewer
777 measurements, *Atmos. Chem. Phys.*, 15, 667-683, doi: 10.5194/acp-15-667-2015, 2015.
- 778 Bak, J., Liu, X., Wei, J. C., Pan, L. L., Chance, K., and Kim, J. H.: Improvement of OMI ozone
779 profile retrievals in the upper troposphere and lower stratosphere by the use of a tropopause-
780 based ozone profile climatology, *Atmos. Meas. Tech.*, 6, 2239-2254, doi: 10.5194/amt-6-2239-
781 2013, 2013b.
- 782 Bhartia, P. K., and Wellemeyer, C. G.: TOMS-V8 total ozone algorithm, in: *OMI Algorithm*
783 *Theoretical Basis Document*, edited by: Bhartia, P. K., Greenbelt, 2002.
- 784 Cai, Z., Liu, Y., Liu, X., Chance, K., Nowlan, C. R., Lang, R., Munro, R., and Suleiman, R.:
785 Characterization and correction of Global Ozone Monitoring Experiment 2 ultraviolet
786 measurements and application to ozone profile retrievals, *J. Geophys. Res.*, 117, doi:
787 10.1029/2011jd017096, 2012.
- 788 Caudill, T. R., Flittner, D. E., Herman, B. M., Torres, O., and McPeters, R. D.: Evaluation of the
789 pseudo-spherical approximation for backscattered ultraviolet radiances and ozone retrieval, *J.*
790 *Geophys. Res.*, 102, 3881-3890, 1997.
- 791 Claas, J.: *OMI and AURA: Status, Instrument, Spacecraft and Operations*, OMI Science Meeting
792 Meeting, De Bilt, the Netherlands, 2014.
- 793 Deshler, T., Mercer, J. L., Smit, H. G. J., Stubi, R., Levrat, G., Johnson, B. J., Oltmans, S. J.,
794 Kivi, R., Thompson, A. M., Witte, J., Davies, J., Schmidlin, F. J., Brothers, G., and Sasaki, T.:
795 Atmospheric comparison of electrochemical cell ozonesondes from different manufacturers, and
796 with different cathode solution strengths: The Balloon Experiment on Standards for
797 Ozonesondes, *J. Geophys. Res.*, 113, doi: 10.1029/2007JD008975, 2008.
- 798 Hassler, B., Petropavlovskikh, I., Staehelin, J., August, T., Bhartia, P. K., Clerbaux, C.,
799 Degenstein, D., Mazière, M. D., Dinelli, B. M., Dudhia, A., Dufour, G., Frith, S. M., Froidevaux,
800 L., Godin-Beekmann, S., Granville, J., Harris, N. R. P., Hoppel, K., Hubert, D., Kasai, Y.,
801 Kurylo, M. J., Kyrölä, E., Lambert, J. C., Levelt, P. F., McElroy, C. T., McPeters, R. D., Munro,
802 R., Nakajima, H., Parrish, A., Raspollini, P., Remsberg, E. E., Rosenlof, K. H., Rozanov, A.,
803 Sano, T., Sasano, Y., Shiotani, M., Smit, H. G. J., Stiller, G., Tamminen, J., Tarasick, D. W.,
804 Urban, J., van der A, R. J., Veefkind, J. P., Vigouroux, C., von Clarmann, T., von Savigny, C.,
805 Walker, K. A., Weber, M., Wild, J., and Zawodny, J. M.: Past changes in the vertical distribution
806 of ozone - Part 1: Measurement techniques, uncertainties and availability, *Atmos. Meas. Tech.*,
807 7, 1395-1427, doi: 10.5194/amt-7-1395-2014, 2014.

808 Hayashida, S., Liu, X., Ono, A., Yang, K., and Chance, K.: Observation of ozone enhancement
809 in the lower troposphere over East Asia from a space-borne ultraviolet spectrometer, *Atmos.*
810 *Chem. Phys.*, 15, 9865-9881, doi: 10.5194/acp-15-9865-2015, 2015.

811 Huang, G., Liu, X., Chance, K., Yang, K., and Cai, Z.: Validation of 10-year SAO OMI Ozone
812 Profile (PROFOZ) Product Using Aura MLS Measurements, *Atmos. Meas. Tech. Discuss.*,
813 2017, 1-25, doi: 10.5194/amt-2017-92, 2017.

814 Huang, G., Newchurch, M. J., Kuang, S., Buckley, P. I., Cantrell, W., and Wang, L.: Definition
815 and determination of ozone laminae using Continuous Wavelet Transform (CWT) analysis,
816 *Atmos. Environ.*, 104, 125-131, doi: 10.1016/j.atmosenv.2014.12.027, 2015.

817 Johnson, B. J.: Electrochemical concentration cell (ECC) ozonesonde pump efficiency
818 measurements and tests on the sensitivity to ozone of buffered and unbuffered ECC sensor
819 cathode solutions, *IEEE T. Geosci. Remote.*, 107, 4393, doi: 10.1029/2001jd000557, 2002.

820 Kim, P. S., Jacob, D. J., Liu, X., Warner, J. X., Yang, K., Chance, K., Thouret, V., and Nedelec,
821 P.: Global ozone–CO correlations from OMI and AIRS: constraints on tropospheric ozone
822 sources, *Atmos. Chem. Phys.*, 13, 9321-9335, doi: 10.5194/acp-13-9321-2013, 2013.

823 Kivi, R., Kyrö, E., Turunen, T., Harris, N. R. P., von der Gathen, P., Rex, M., Andersen, S. B.,
824 and Wohltmann, I.: Ozonesonde observations in the Arctic during 1989–2003: Ozone variability
825 and trends in the lower stratosphere and free troposphere, *J. Geophys. Res.*, 112, doi:
826 10.1029/2006JD007271, 2007.

827 Komhyr, W. D.: Operations on handbook-Ozone measurements to 40-km altitude with model 4A
828 electrochemical concentration cell (ECC) ozonesondes, NOAA Tech. Memo. ERLARL-149 Air
829 Resour. Lab., Boulder, CO, 49 pp., 1986.

830 Komhyr, W. D., Connor, B. J., McDermid, I. S., McGee, T. J., Parrish, A. D., and Margitan, J. J.:
831 Comparison of STOIC 1989 ground-based lidar, microwave spectrometer, and Dobson
832 spectrophotometer Umkehr ozone profiles with ozone profiles from balloon-borne
833 electrochemical concentration cell ozonesondes, *J. Geophys. Res.*, 100, 9273-9282, 1995.

834 Kroon, M., de Haan, J. F., Veeffkind, J. P., Froidevaux, L., Wang, R., Kivi, R., and Hakkarainen,
835 J. J.: Validation of operational ozone profiles from the Ozone Monitoring Instrument, *J.*
836 *Geophys. Res.*, 116, D18305, doi: 10.1029/2010jd015100, 2011.

837 Lal, S., Venkataramani, S., Srivastava, S., Gupta, S., Mallik, C., Naja, M., Sarangi, T., Acharya,
838 Y. B., and Liu, X.: Transport effects on the vertical distribution of tropospheric ozone over the
839 tropical marine regions surrounding India, *J. Geophys. Res.*, 118, 1513-1524, 2013.

840 Levelt, P. F., van den Oord, G. H. J., Dobber, M. R., Malkki, A., Visser, H., de Vries, J.,
841 Stammes, P., Lundell, J. O. V., and Saari, H.: The Ozone Monitoring Instrument, *IEEE T.*
842 *Geosci. Remote.*, 44, 1093-1101, 2006.

843 Liu, G., Liu, J., Tarasick, D. W., Fioletov, V. E., Jin, J. J., Moeini, O., Liu, X., Sioris, C. E., and
844 Osman, M.: A global tropospheric ozone climatology from trajectory-mapped ozone soundings,
845 *Atmos. Chem. Phys.*, 13, 10659-10675, doi: 10.5194/acp-13-10659-2013, 2013.

846 Liu, G., Tarasick, D. W., Fioletov, V. E., Sioris, C. E., and Rochon, Y. J.: Ozone correlation
847 lengths and measurement uncertainties from analysis of historical ozonesonde data in North
848 America and Europe, *J. Geophys. Res.*, 114, doi: 10.1029/2008JD010576, 2009.

849 Liu, X., Bhartia, P. K., Chance, K., Froidevaux, L., Spurr, R. J. D., and Kurosu, T. P.: Validation
850 of Ozone Monitoring Instrument (OMI) ozone profiles and stratospheric ozone columns with
851 Microwave Limb Sounder (MLS) measurements, *Atmos. Chem. Phys.*, 10, 2539-2549, doi:
852 10.5194/acp-10-2539-2010, 2010a.

853 Liu, X., Bhartia, P. K., Chance, K., Spurr, R. J. D., and Kurosu, T. P.: Ozone profile retrievals
854 from the Ozone Monitoring Instrument, *Atmos. Chem. Phys.*, 10, 2521-2537, doi: 10.5194/acp-
855 10-2521-2010, 2010b.

856 Liu, X., Chance, K., and Kurosu, T. P.: Improved ozone profile retrievals from GOME data with
857 degradation correction in reflectance, *Atmos. Chem. Phys.*, 7, 1575-1583, 2007.

858 Liu, X., Chance, K., Sioris, C. E., Kurosu, T. P., and Newchurch, M. J.: Intercomparison of
859 GOME, ozonesonde, and SAGE II measurements of ozone: Demonstration of the need to
860 homogenize available ozonesonde data sets, *J. Geophys. Res.*, 111, D114305, doi:
861 10.1029/2005jd006718, 2006a.

862 Liu, X., Chance, K., Sioris, C. E., Kurosu, T. P., Spurr, R. J. D., Martin, R. V., Fu, T.-M., Logan,
863 J. A., Jacob, D. J., Palmer, P. I., Newchurch, M. J., Megretskaya, I. A., and Chatfield, R. B.: First
864 directly retrieved global distribution of tropospheric column ozone from GOME: Comparison
865 with the GEOS-CHEM model, *J. Geophys. Res.*, 111, doi: 10.1029/2005JD006564, 2006b.

866 Liu, X., Chance, K., Sioris, C. E., Spurr, R. J. D., Kurosu, T. P., Martin, R. V., and Newchurch,
867 M. J.: Ozone profile and tropospheric ozone retrievals from the Global Ozone Monitoring
868 Experiment: Algorithm description and validation, *J. Geophys. Res.*, 110, D20307, doi:
869 10.1029/2005jd006240, 2005.

870 McPeters, R. D., Labow, G. J., and Logan, J. A.: Ozone climatological profiles for satellite
871 retrieval algorithms, *J. Geophys. Res.*, 112, D05308, doi: 10.1029/2005jd006823, 2007.

872 Morris, G. A., Labow, G., Akimoto, H., Takigawa, M., Fujiwara, M., Hasebe, F., Hirokawa, J.,
873 and Koide, T.: On the use of the correction factor with Japanese ozonesonde data, *Atmos. Chem.*
874 *Phys.*, 13, 1243-1260, doi: 10.5194/acp-13-1243-2013, 2013.

875 Pittman, J. V., Pan, L. L., Wei, J. C., Irion, F. W., Liu, X., Maddy, E. S., Barnett, C. D., Chance,
876 K., and Gao, R.-S.: Evaluation of AIRS, IASI, and OMI ozone profile retrievals in the
877 extratropical tropopause region using in situ aircraft measurements, *J. Geophys. Res.*, 114,
878 24109, doi: 10.1029/2009jd012493, 2009.

879 Saunio, M., Emmons, L., Lamarque, J. F., Tilmes, S., Wespes, C., Thouret, V., and Schultz, M.:
880 Impact of sampling frequency in the analysis of tropospheric ozone observations, *Atmos. Chem.*
881 *Phys.*, 12, 6757-6773, doi: 10.5194/acp-12-6757-2012, 2012.

882 Sellitto, P., Bojkov, B. R., Liu, X., Chance, K., and Del Frate, F.: Tropospheric ozone column
883 retrieval at northern mid-latitudes from the Ozone Monitoring Instrument by means of a neural
884 network algorithm, *Atmospheric Measurement Techniques*, 4, 2375-2388, 2011.

885 Smit, H. G. J., Straeter, W., Johnson, B. J., Oltmans, S. J., Davies, J., Tarasick, D. W., Hoegger,
886 B., Stubi, R., Schmidlin, F. J., Northam, T., Thompson, A. M., Witte, J. C., Boyd, I., and Posny,
887 F.: Assessment of the performance of ECC-ozonesondes under quasi-flight conditions in the
888 environmental simulation chamber: Insights from the Juelich Ozone Sonde Intercomparison
889 Experiment (JOSIE), *J. Geophys. Res.*, 112, 19306, 2007.

890 Tarasick, D. W., Jin, J. J., Fioletov, V. E., Liu, G., Thompson, A. M., Oltmans, S. J., Liu, J.,
891 Sioris, C. E., Liu, X., Cooper, O. R., Dann, T., and Thouret, V.: High-resolution tropospheric
892 ozone fields for INTEX and ARCTAS from IONS ozonesondes, *J. Geophys. Res.*, 115, 20301,
893 doi: doi: 10.1029/2009JD012918, 2010.

894 Thompson, A. M., Miller, S. K., Tilmes, S., Kollonige, D. W., Witte, J. C., Oltmans, S. J.,
895 Johnson, B. J., Fujiwara, M., Schmidlin, F. J., Coetzee, G. J. R., Komala, N., Maata, M., bt
896 Mohamad, M., Nguyo, J., Mutai, C., Ogino, S. Y., Da Silva, F. R., Leme, N. M. P., Posny, F.,
897 Scheele, R., Selkirk, H. B., Shiotani, M., Stübi, R., Levrat, G., Calpini, B., Thouret, V., Tsuruta,
898 H., Canossa, J. V., Vömel, H., Yonemura, S., Diaz, J. A., Tan Thanh, N. T., and Thuy Ha, H. T.:
899 Southern Hemisphere Additional Ozonesondes (SHADOZ) ozone climatology (2005-2009):
900 Tropospheric and tropical tropopause layer (TTL) profiles with comparisons to OMI-based
901 ozone products, *J. Geophys. Res.*, 117, doi: 10.1029/2011jd016911, 2012.

902 Thompson, A. M., Stauffer, R. M., Miller, S. K., Martins, D. K., Joseph, E., Weinheimer, A. J.,
903 and Diskin, G. S.: Ozone profiles in the Baltimore-Washington region (2006-2011): satellite
904 comparisons and DISCOVER-AQ observations, *J Atmos Chem*, 72, 393-422, doi:
905 10.1007/s10874-014-9283-z, 2015.

906 Thompson, A. M., Stone, J. B., Witte, J. C., Miller, S. K., Oltmans, S. J., Kucsera, T. L., Ross,
907 K. L., Pickering, K. E., Merrill, J. T., Forbes, G., Tarasick, D. W., Joseph, E., Schmidlin, F. J.,
908 McMillan, W. W., Warner, J., Hints, E. J., and Johnson, J. E.: Intercontinental Chemical
909 Transport Experiment Ozonesonde Network Study (IONS) 2004: 2. Tropospheric ozone budgets
910 and variability over northeastern North America, *J. Geophys. Res.*, 112, doi:
911 10.1029/2006jd007670, 2007a.

912 Thompson, A. M., Stone, J. B., Witte, J. C., Miller, S. K., Pierce, R. B., Chatfield, R. B.,
913 Oltmans, S. J., Cooper, O. R., Loucks, A. L., Taubman, B. F., Johnson, B. J., Joseph, E.,
914 Kucsera, T. L., Merrill, J. T., Morris, G. A., Hersey, S., Forbes, G., Newchurch, M. J.,
915 Schmidlin, F. J., Tarasick, D. W., Thouret, V., and Cammas, J.-P.: Intercontinental Chemical
916 Transport Experiment Ozonesonde Network Study (IONS) 2004: 1. Summertime upper
917 troposphere/lower stratosphere ozone over northeastern North America, *J. Geophys. Res.*, 112,
918 doi: 10.1029/2006jd007441, 2007b.

919 Thompson, A. M., Witte, J. C., Smit, H. G. J., Oltmans, S. J., Johnson, B. J., Kirchhoff, V. W. J.
920 H., and Schmidlin, F. J.: Southern Hemisphere Additional Ozonesondes (SHADOZ) 1998–2004
921 tropical ozone climatology: 3. Instrumentation, station-to-station variability, and evaluation with
922 simulated flight profiles, *J. Geophys. Res.*, 112, doi: 10.1029/2005jd007042, 2007c.

923 Thompson, A. M., Yorks, J. E., Miller, S. K., Witte, J. C., Dougherty, K. M., Morris, G. A.,
924 Baumgardner, D., Ladino, L., and Rappenglück, B.: Tropospheric ozone sources and wave
925 activity over Mexico City and Houston during MILAGRO/Intercontinental Transport

926 Experiment (INTEX-B) Ozonesonde Network Study, 2006 (IONS-06), *Atmos. Chem. Phys.*, 8,
927 5113-5125, 2008.

928 Toon, O. B., Maring, H., Dibb, J., Ferrare, R., Jacob, D. J., Jensen, E. J., Luo, Z. J., Mace, G. G.,
929 Pan, L. L., Pfister, L., Rosenlof, K. H., Redemann, J., Reid, J. S., Singh, H. B., Thompson, A.
930 M., Yokelson, R., Minnis, P., Chen, G., Jucks, K. W., and Pszenny, A.: Planning,
931 implementation, and scientific goals of the Studies of Emissions and Atmospheric Composition,
932 Clouds and Climate Coupling by Regional Surveys (SEAC4RS) field mission, *J. Geophys. Res.*,
933 121, 4967-5009, doi: 10.1002/2015jd024297, 2016.

934 van Oss, R. F., Voors, R. H. M., and Spurr, R. J. D.: Ozone profile algorithm, in: OMI Algorithm
935 Theoretical Basis Document, Volume II: OMI ozone products, edited by: Bhartia, P. K.,
936 Greenbelt, MD, 51-73, 2001.

937 Vasilkov, A., Joiner, J., Spurr, R., Bhartia, P. K., Levelt, P., and Stephens, G.: Evaluation of the
938 OMI cloud pressures derived from rotational Raman scattering by comparisons with other
939 satellite data and radiative transfer simulations, *J. Geophys. Res.-Atmos.*, 113, n/a-n/a, doi:
940 10.1029/2007JD008689, 2008.

941 Veefkind, J. P., de Haan, J. F., Brinksma, E. J., Kroon, M., and Levelt, P. F.: Total Ozone From
942 the Ozone Monitoring Instrument (OMI) Using the DOAS Technique, *IEEE T. Geosci. Remote.*,
943 44, 1239-1244, 2006.

944 Wang, L., Newchurch, M. J., Biazar, A., Liu, X., Kuang, S., Khan, M., and Chance, K.:
945 Evaluating AURA/OMI ozone profiles using ozonesonde data and EPA surface measurements
946 for August 2006, *Atmos. Environ.*, 45, 5523-5530, doi: 10.1016/j.atmosenv.2011.06.012, 2011.

947 WMO: SPARC/IO3C/GAW Assessment of trends in the vertical distribution of ozone,
948 GenevaRep. 43, 1998.

949 Worden, H. M., Logan, J. A., Worden, J. R., Beer, R., Bowman, K., Clough, S. A., Eldering, A.,
950 Fisher, B. M., Gunson, M. R., Herman, R. L., Kulawik, S. S., Lampel, M. C., Luo, M.,
951 Megretskaia, I. A., Osterman, G. B., and Shephard, M. W.: Comparisons of Tropospheric
952 Emission Spectrometer (TES) ozone profiles to ozonesondes: Methods and initial results, *J.*
953 *Geophys. Res.*, 112, doi: 10.1029/2006jd007258, 2007.

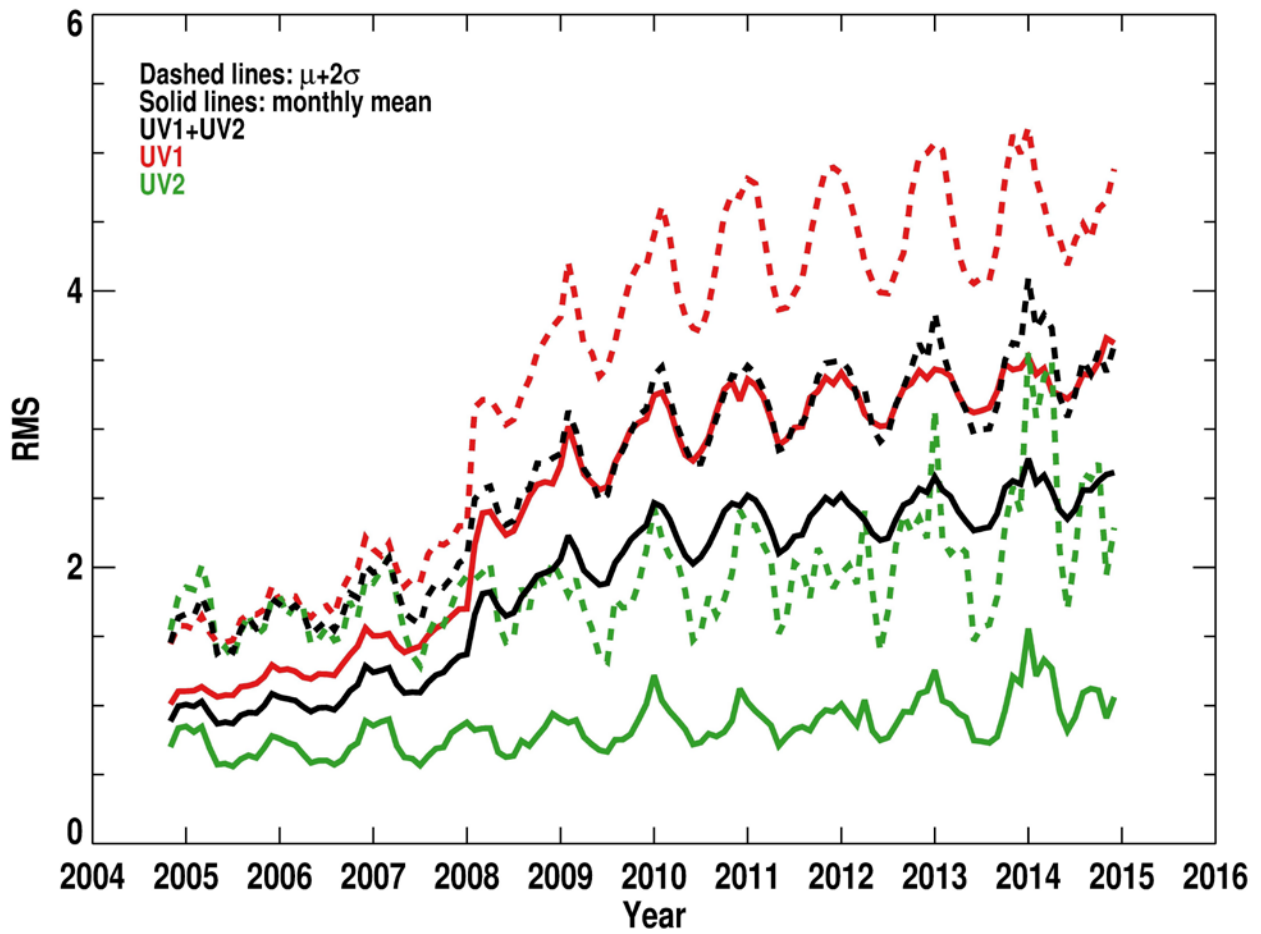
954 Yang, Q., Cunnold, D. M., Wang, H. J., Froidevaux, L., Claude, H., Merrill, J., Newchurch, M.,
955 and Oltmans, S. J.: Midlatitude tropospheric ozone columns derived from the Aura Ozone
956 Monitoring Instrument and Microwave Limb Sounder measurements, *J. Geophys. Res.: Atmos.*,
957 112, D20305, doi: doi: 10.1029/2007JD008528, 2007.

958 Ziemke, J. R., Olsen, M. A., Witte, J. C., Douglass, A. R., Strahan, S. E., Wargan, K., Liu, X.,
959 Schoeberl, M. R., Yang, K., Kaplan, T. B., Pawson, S., Duncan, B. N., Newman, P. A., Bhartia,
960 P. K., and Heney, M. K.: Assessment and applications of NASA ozone data products derived
961 from Aura OMI/MLS satellite measurements in context of the GMI chemical transport model, *J.*
962 *Geophys. Res.*, 119, 5671-5699, doi: 10.1002/2013jd020914, 2014.

963

964

966

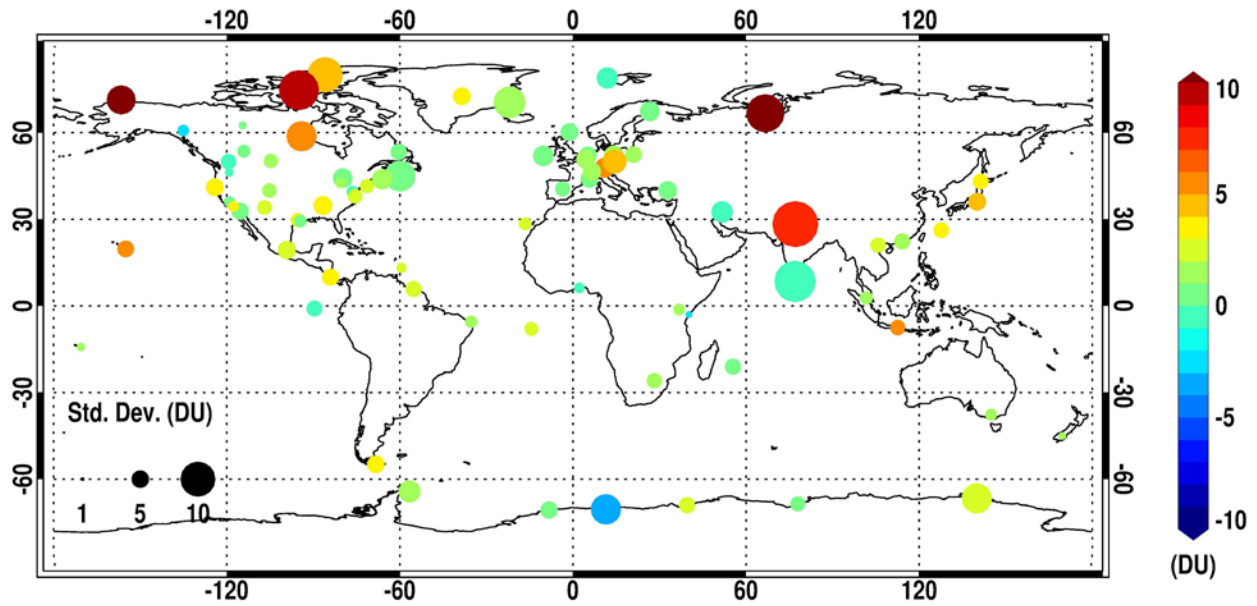


967

968 **Figure 1** Variation of monthly mean OMI RMS (defined as Root Mean Square of the ratio of
969 radiance residuals to assumed radiance errors). The dashed and solid lines represent respectively
970 the monthly mean RMS, and the sum of monthly mean plus its two standard deviations that is set
971 as the RMS threshold for data screening.

972

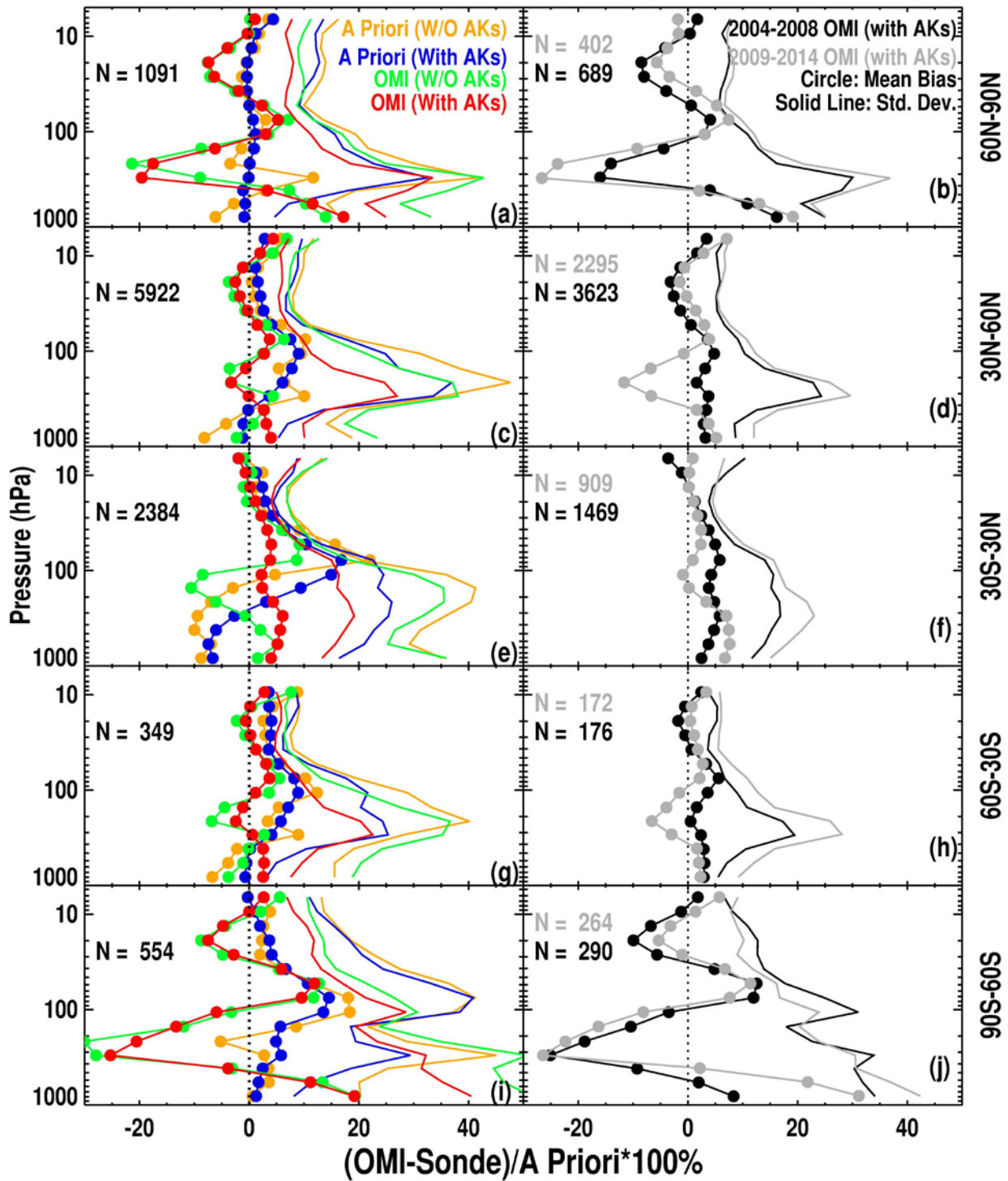
973



974

975 **Figure 2** The distribution of ozonesonde stations in this study. The color represents the mean biases
976 between OMI and ozonesonde tropospheric ozone columns (TOCs) at each station (if the number of
977 OMI and ozonesonde pairs is more than 10), and the dot size represents the standard deviation.

978



980

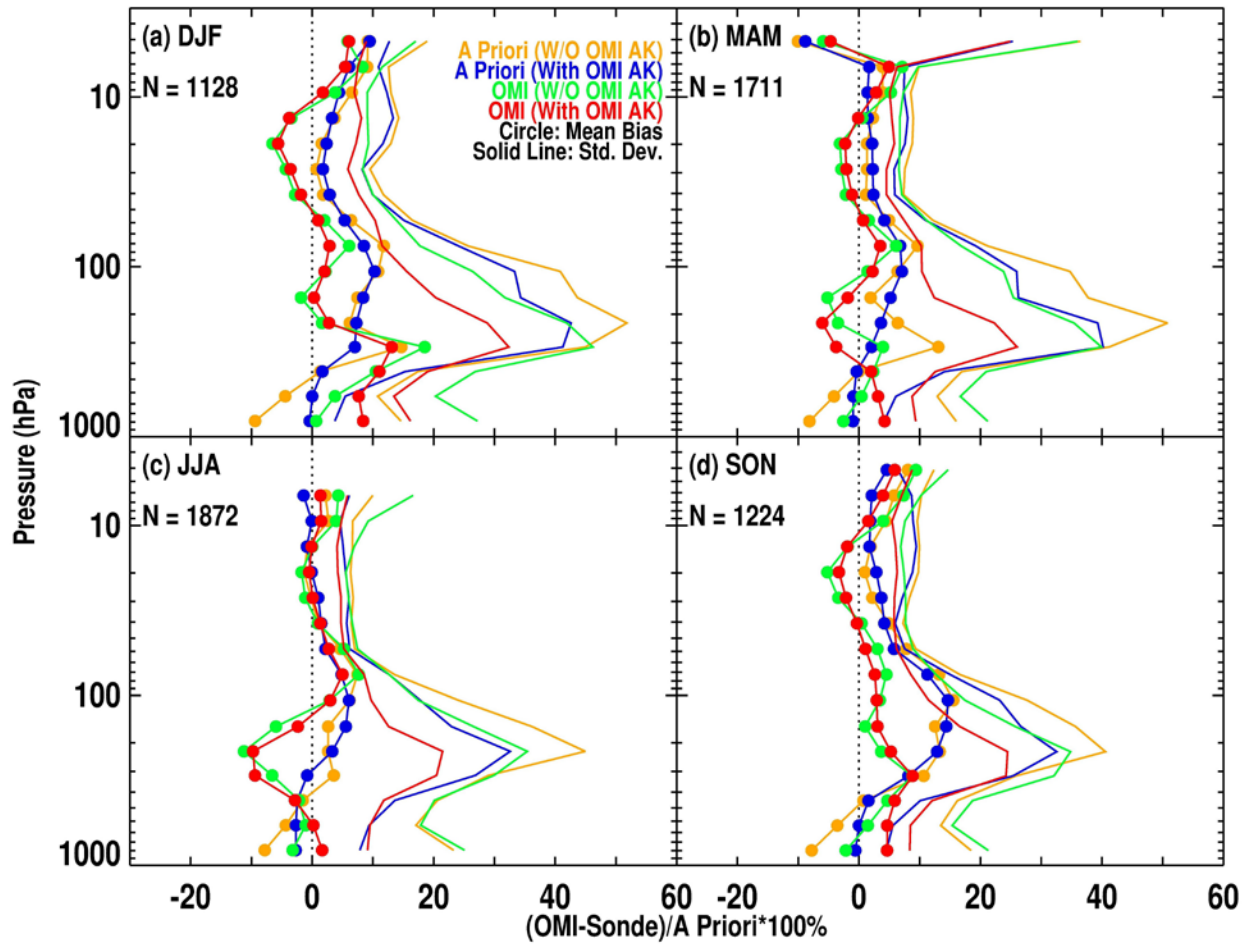
981 Figure 3 Mean relative biases in ozone (line with circles) and corresponding standard deviations
 982 (solid lines) between OMI retrieval/a priori and ozonesondes with and without applying OMI
 983 retrieval averaging kernels (i.e., with AKs, and W/O AKs in red and green for comparing retrievals

984 and in blue and yellow for comparing a priori) for five different latitude bands. The left panels
985 show the comparison using 10 years of OMI data (2004-2014), and the right panels show the
986 comparison between OMI retrieval and ozonesonde with OMI AKs for before and after the
987 occurrence of serious OMI row anomaly (RA), i.e., pre-RA (2004-2008) in black and post-RA
988 (2009-2014) in gray, respectively. The number (N) of OMI/ozonesonde coincidences used in the
989 comparison is indicated in the legends.

990

991

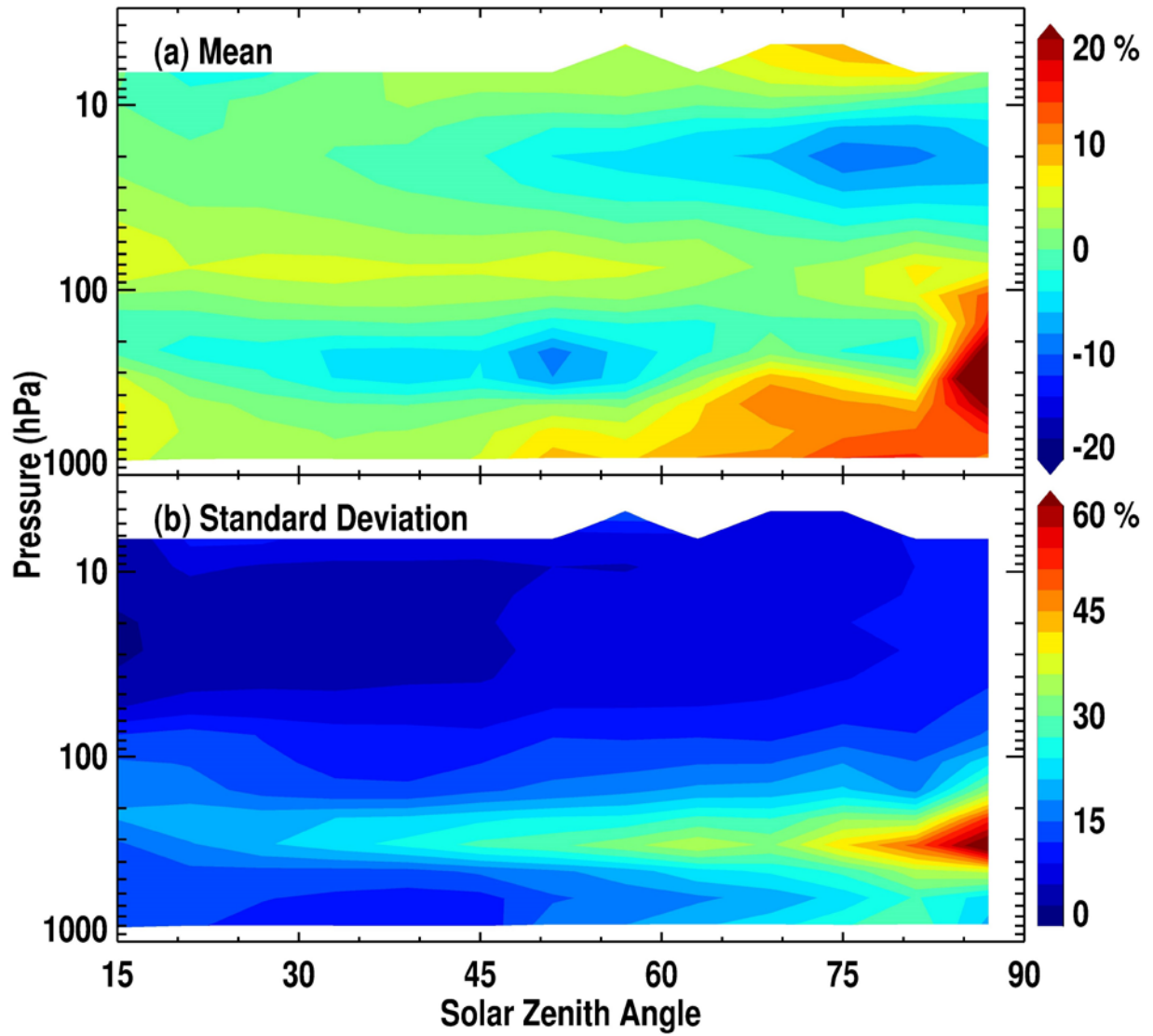
992



993

994 Figure 4 Same as Figure 3c but for each individual season at 30° N-60° N.

995

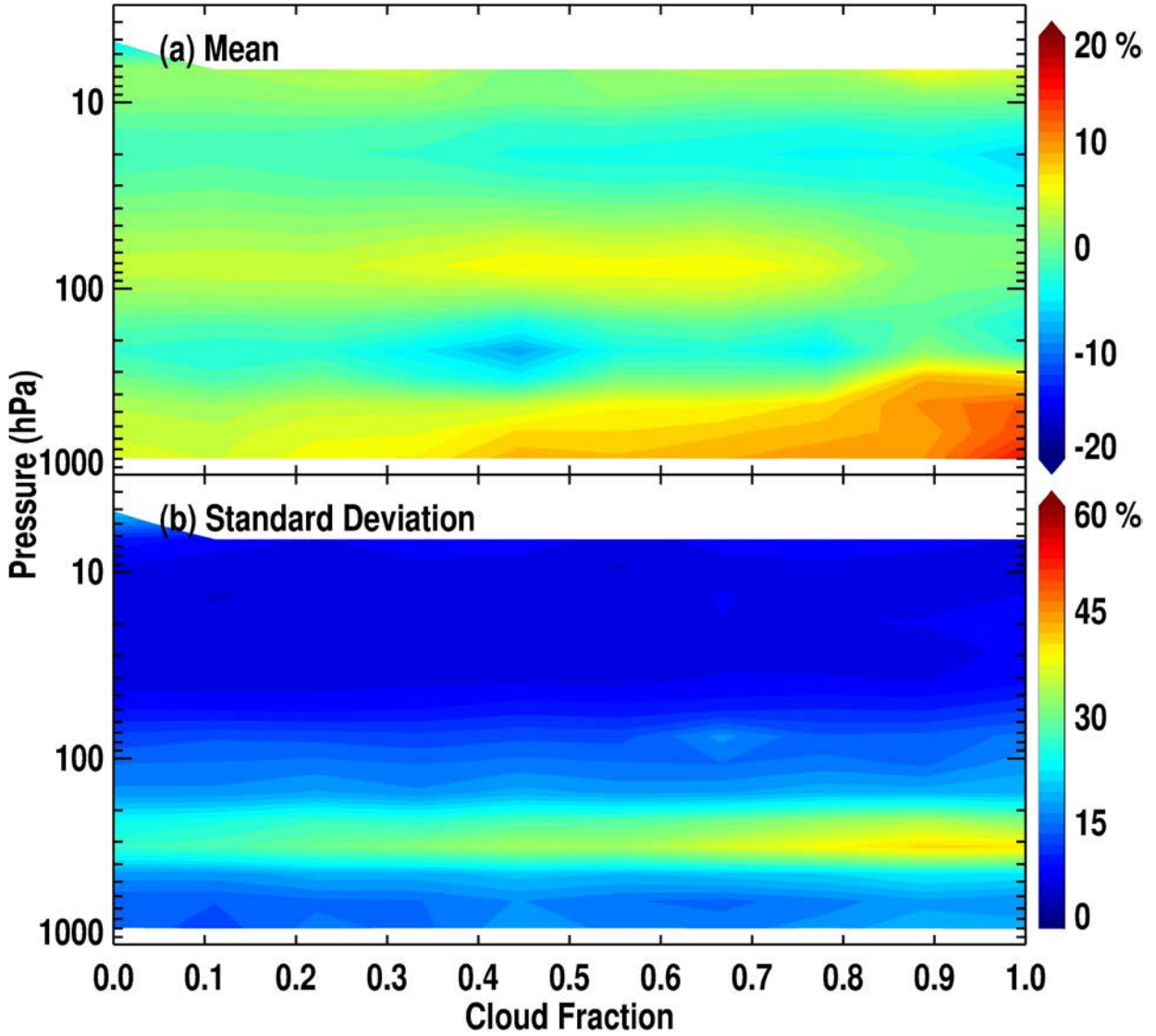


996

997 **Figure 5 Mean relative biases in ozone (a) and standard deviations (b) of the differences between**
 998 **OMI and ozonesonde convolved with OMI AKs as a function of Solar Zenith Angle using all**
 999 **OMI/ozonesonde coincidences during 2004-2014.**

1000

1001



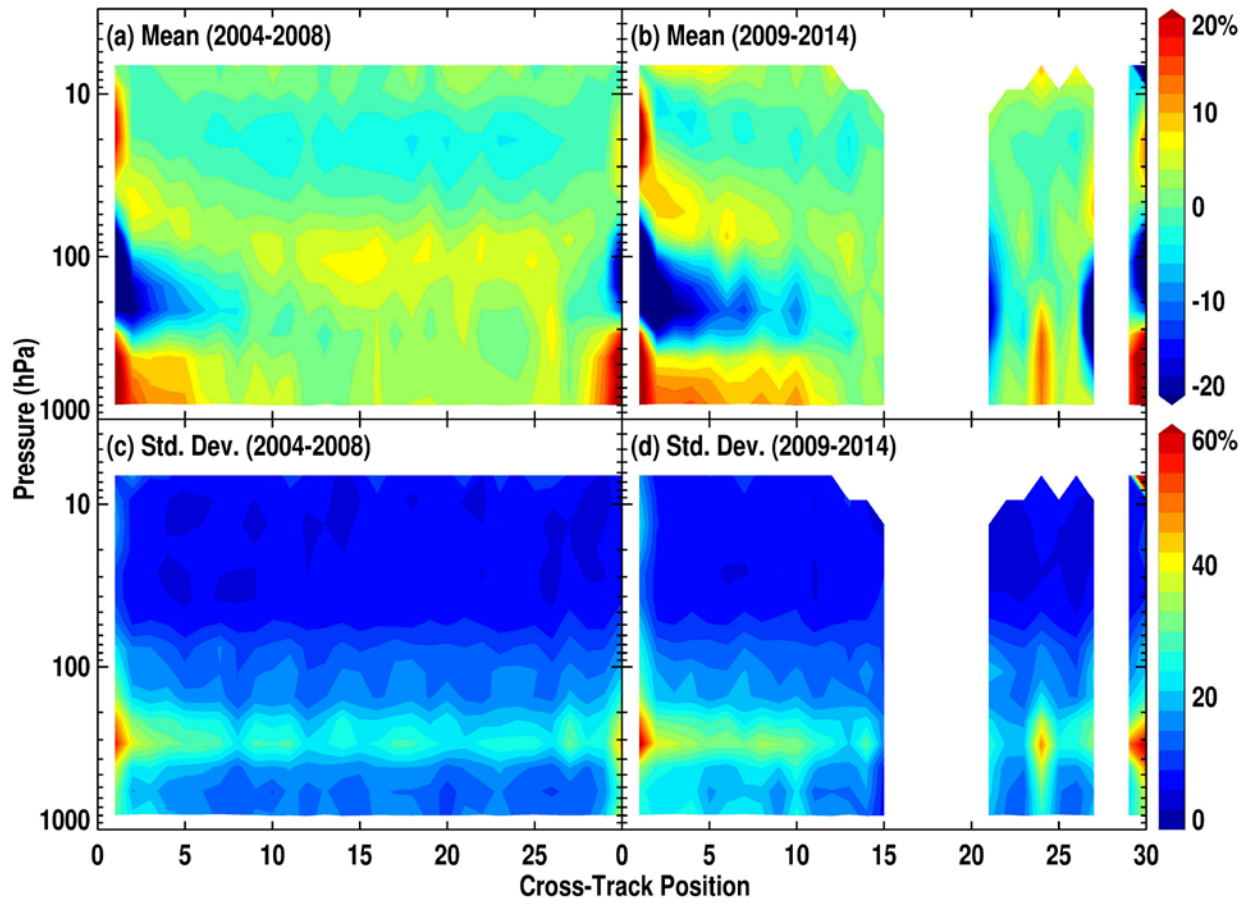
1002

1003 **Figure 6 Same as Figure 5 but as a function of cloud fraction.**

1004

1005

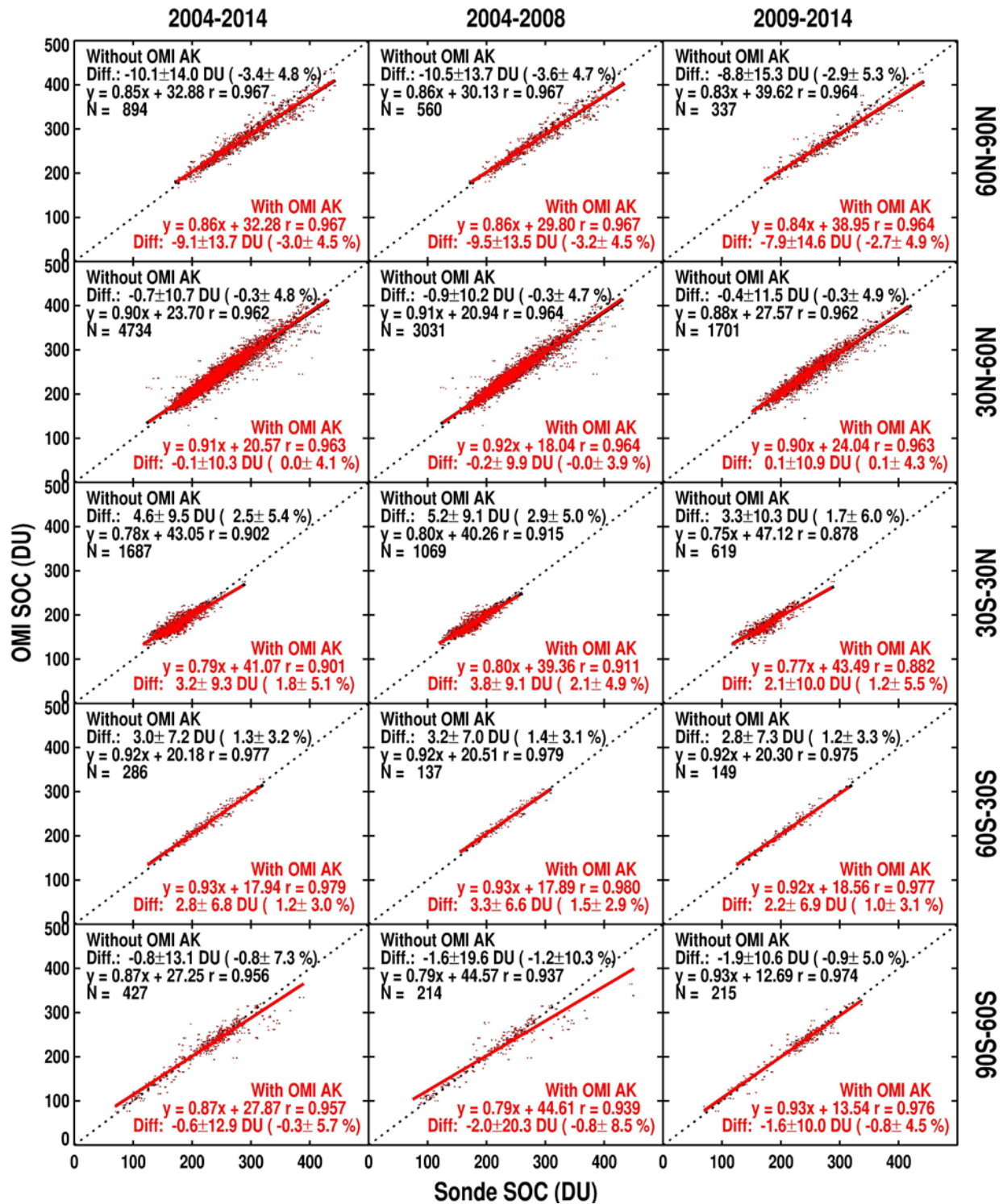
1006



1007

1008 **Figure 7** Same as **Figure 5** but as a function of cross-track position for (left) pre-RA (2004-2008)
1009 and (right) post-RA (2009-2014) periods, respectively.

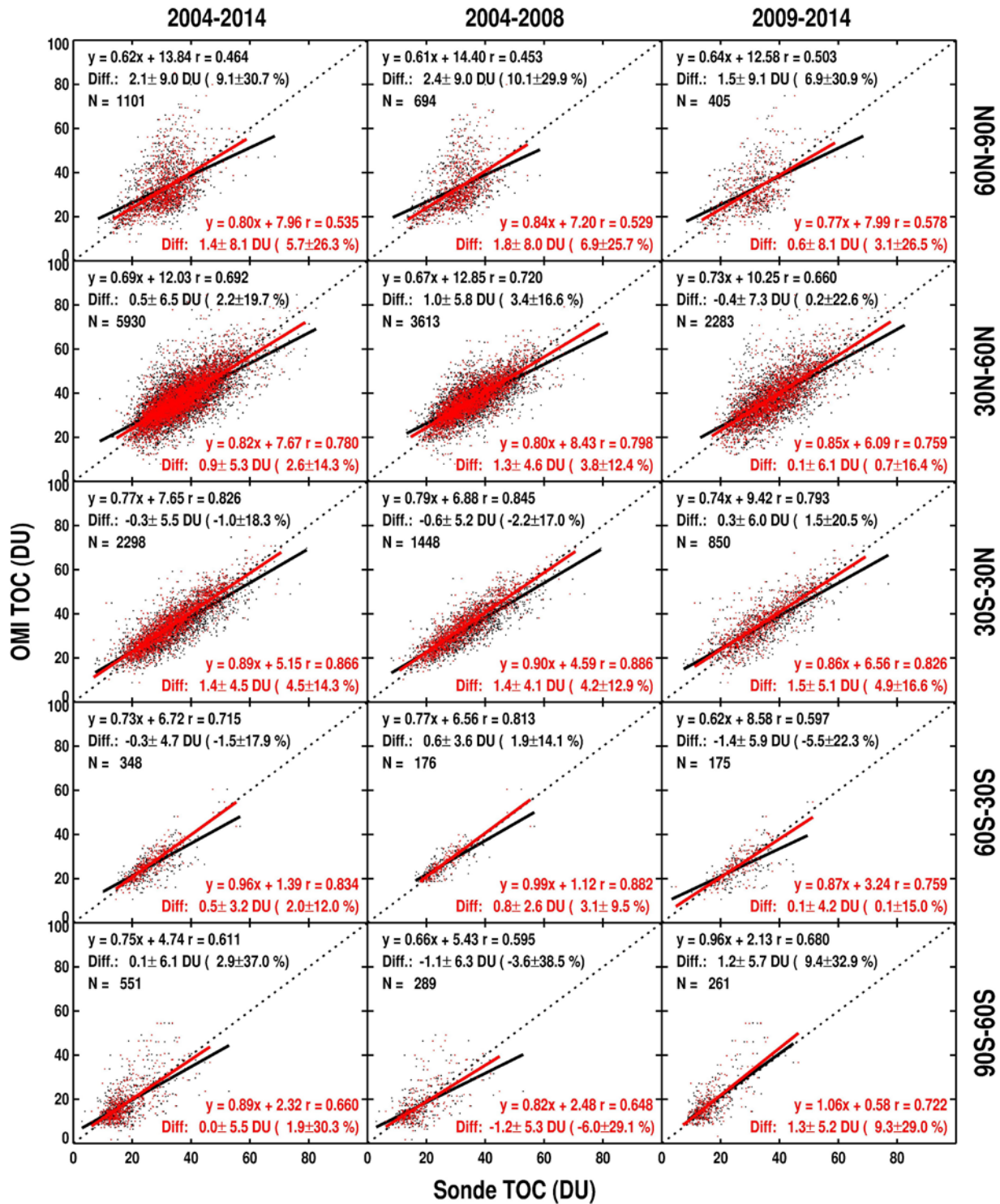
1010



1011

1012 **Figure 8.** Scatter plots of OMI Stratospheric Ozone Columns (SOCs) vs. ozonesonde SOC (DU) without
 1013 (black) and with (red) average kernels for five different latitude bands during 2004-2014 (left), the
 1014 pre-row anomaly (RA) period (i.e., 2004-2008, middle) and the post-RA period (i.e., 2009-2014,
 1015 right), respectively. Comparison statistics including mean biases and standard deviations in both

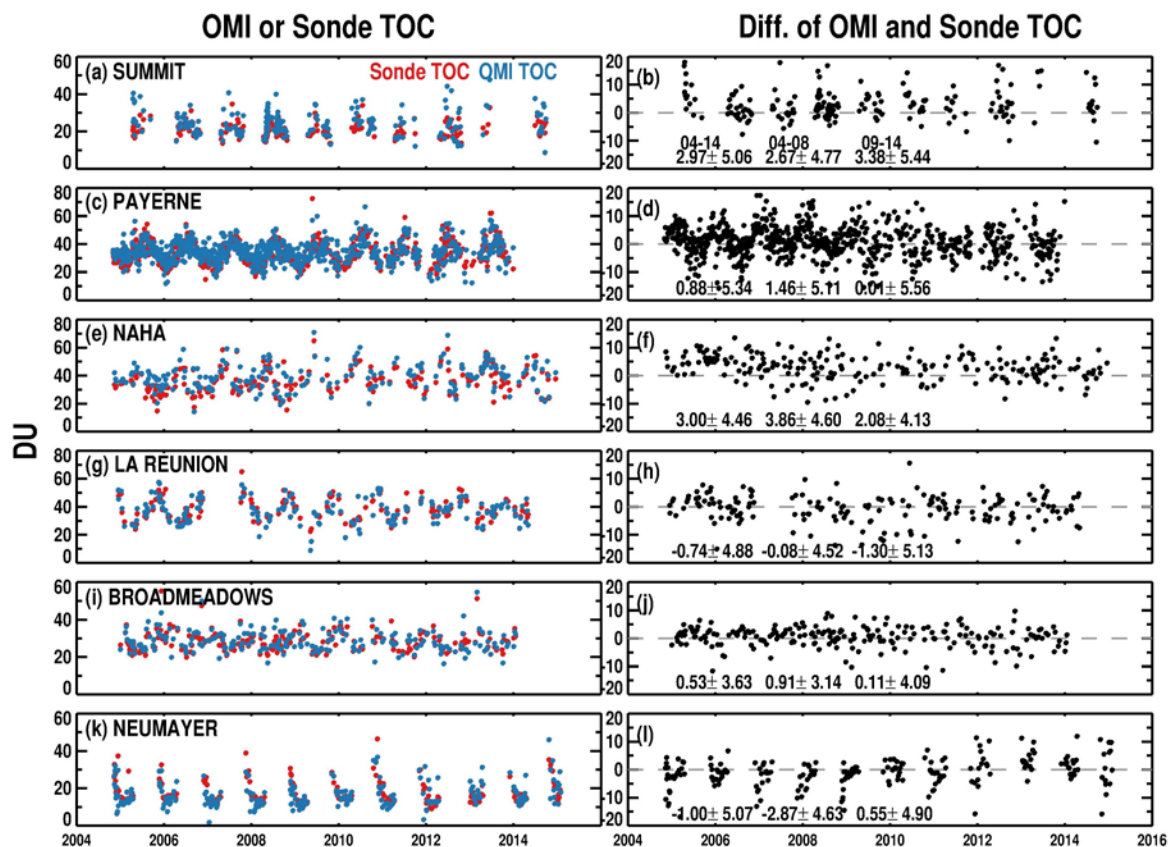
1016 **DU and %, the linear regression and correlation coefficients in DU, and the number of coincidences**
1017 **are shown in the legends.**



1019

1020 **Figure 9.** Similar to Figure 8, but for comparison of Tropospheric Ozone Columns (TOCs).

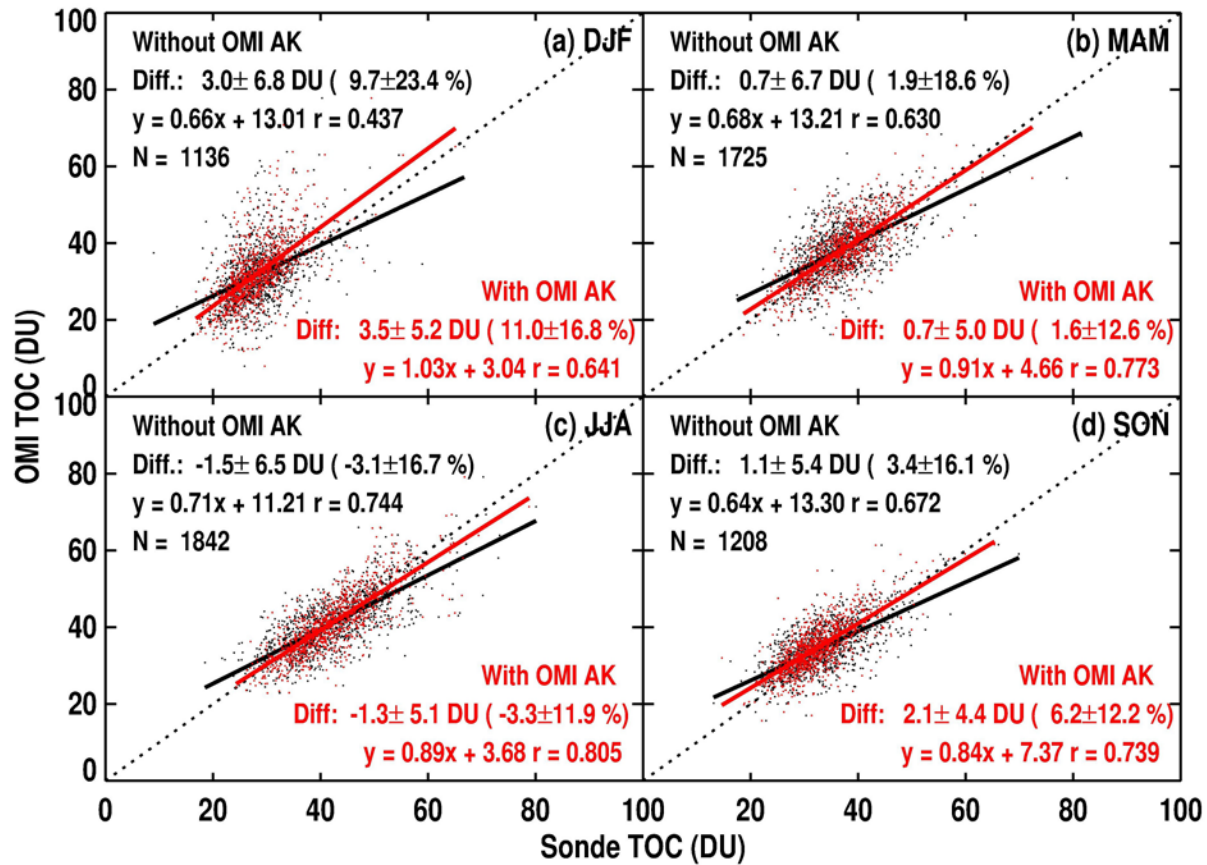
1021



1022

1023 **Figure 10. (Left) Time series of OMI tropospheric ozone columns (TOCs) as green dots and**
 1024 **ozonesonde TOCs (with OMI AKs applied) in Summit (38.48° W, 72.57° N), Payene (6.57° E, 46.49°**
 1025 **N), Naha (127.69° E, 26.21° N), La Réunion (55.48° E, 21.06° S), Broadmeadows (144.95° E, 58.74°**
 1026 **S) and Neumayer (8.27° W, 70.68° S), and (Right) their corresponding differences, including the**
 1027 **mean biases and standard deviations in 2004-2014, pre-RA (2004-2008) and post-RA (2009-2014)**
 1028 **periods, respectively, in the legends.**

1029

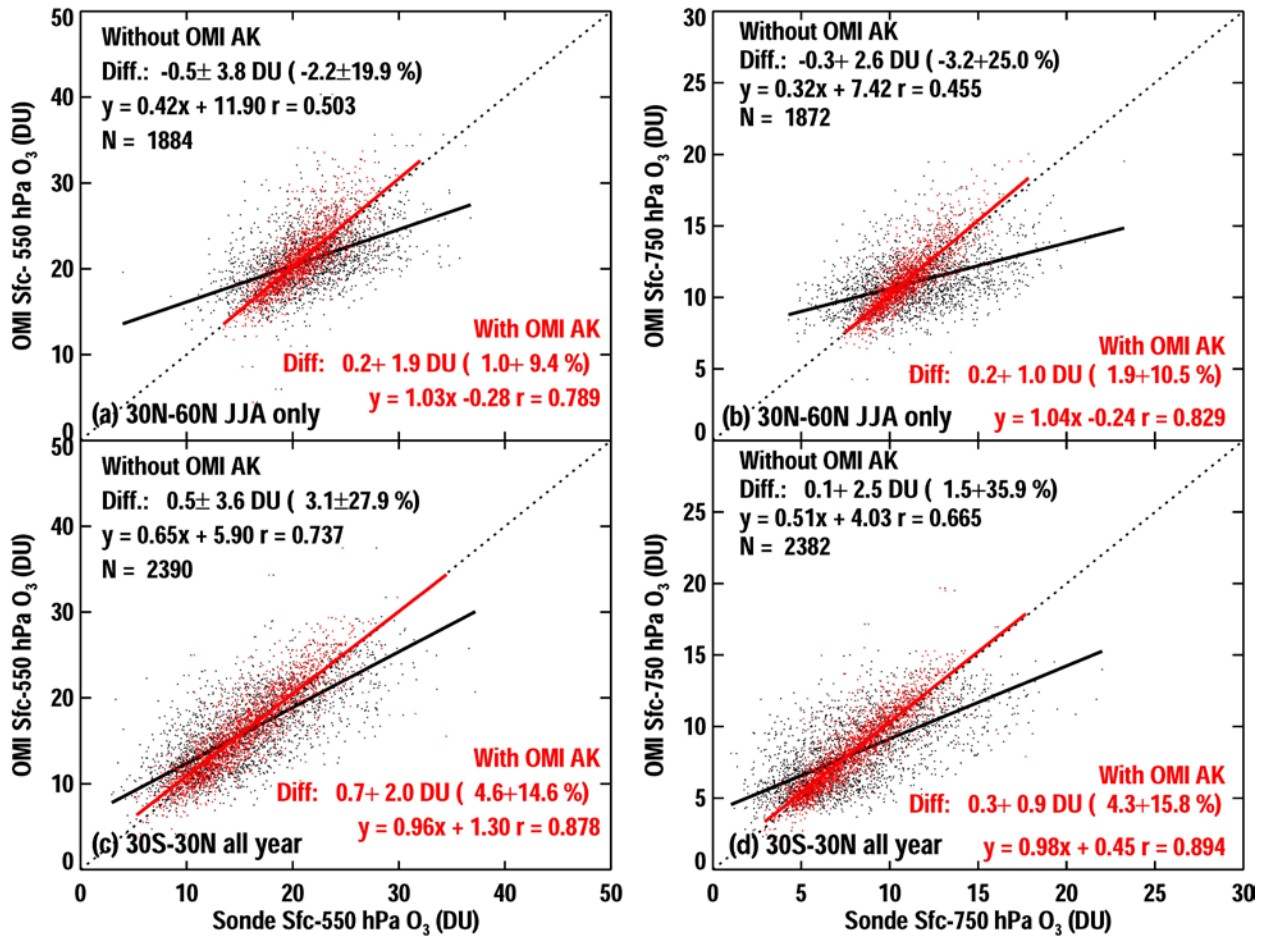


1030

1031 **Figure 11. Similar to Fig. 9 but for different seasons at northern middle latitude during the 2004-**
 1032 **2014 period.**

1033

1034

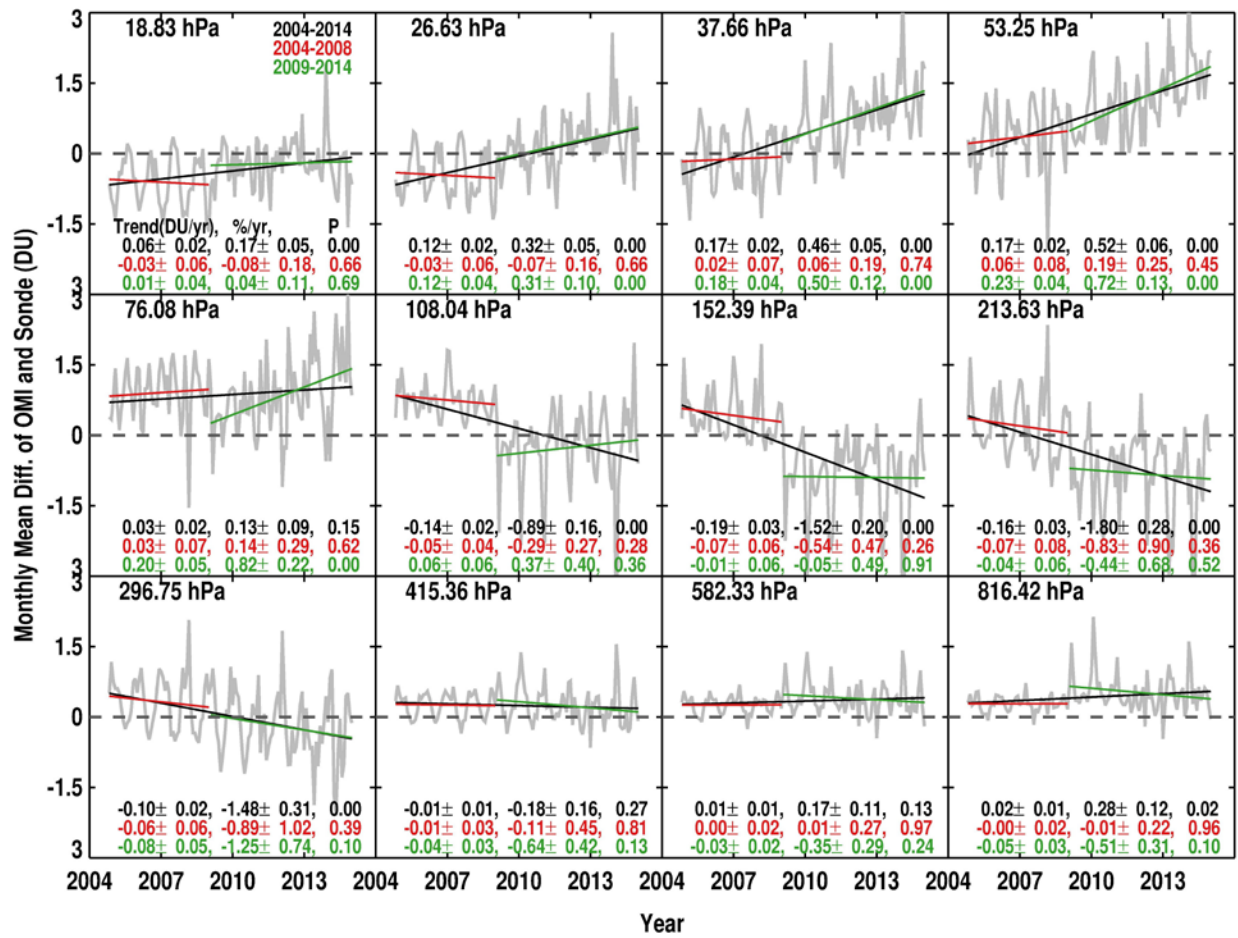


1035

1036 Figure 12. Similar to Fig. 9 but for comparison of lower tropospheric ozone columns during the
1037 2004-2014 period. (a) Surface~550 hPa ozone column and (b) Surface~750 hPa ozone column in 30°
1038 N-60° N during the summer, (c) and (d) same as (a) and (b) but for the tropics.

1039

1040

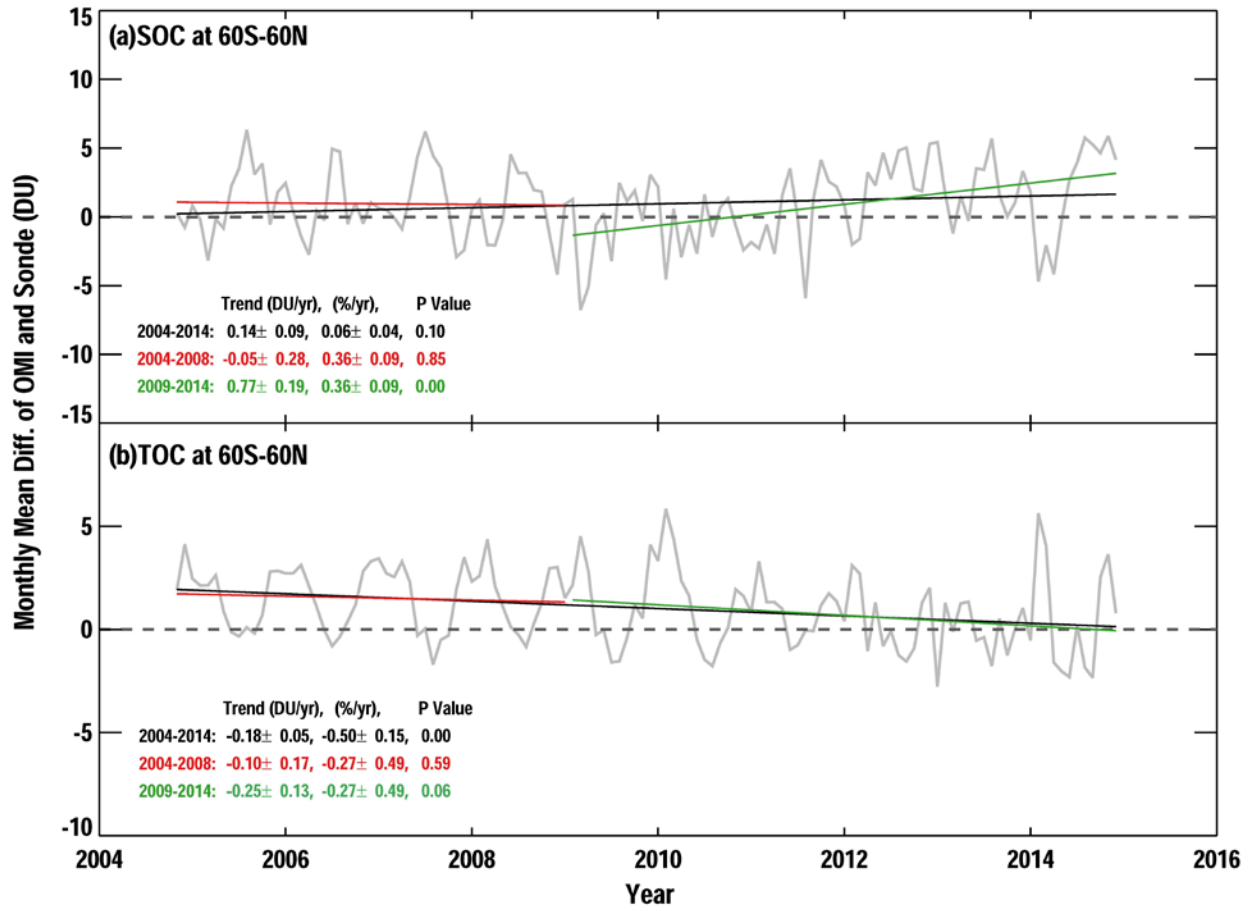


1041

1042 **Figure 13. Monthly mean variation of OMI and ozonesonde mean biases in 60° N-60° S at each**
 1043 **OMI layer. OMI retrieval averaging kernels are applied to ozonesonde data. The black, red and**
 1044 **green lines represent the linear ozone bias trends in 2004-2014, pre-RA (2004-2008) and post-RA**
 1045 **(2009-2014), respectively. The average altitude of each layer is marked on the left corner of each**
 1046 **grid. The trends in DU/yr or % yr and P value for each time period are indicated in the legends.**

1047

1048



1049

1050 Figure 14. Same as Figure 13 but for Stratospheric Ozone Columns (SOCs) and Tropospheric
1051 Ozone Columns (TOCs).